Impacts de la régulation des rivières sur l'apport en CDOM sur la côte est de la baie James

Mémoire présenté

dans le cadre du programme de maîtrise en océanographie

en vue de l'obtention du grade de maître ès sciences

PAR

© AMÉLIE ÉVRARD

Mai 2024

Composition du jury :

Stephanie Kusch, présidente du jury, Université du Québec à Rimouski

Huixiang Xie, directeur de recherche, Université du Québec à Rimouski

Michel Gosselin, codirecteur de recherche, Université du Québec à Rimouski

Céline Guéguen, examinatrice externe, Université de Sherbrooke

Dépôt initial le 29 Février 2024 Dépôt final le 15 Mai 2024

J’aimerais dédier ce mémoire à Charlotte, Olivia, Clémentine, Marilyne, Bernadette, Elliot, Jules, Sophie, Alice, Arnaud, Justine et Renaud.

REMERCIEMENTS

The people from the communities of Chisasibi, Wemindji and Eastmain were incredibly helpful in various aspects of our project. I extend my gratitude to the elders, the boaters, and all those who contributed. It was a pleasure collaborating with you and learning about your culture and the Cree. This has been a significant life experience for me.

Je tiens à remercier Huixiang et Michel pour leur soutien malgré les circonstances inhabituelles qui se sont présentées au cours de ce projet. Je me suis sentie très bien accueillie, merci beaucoup. Virginie Galindo a également été un excellent mentor qui m'a fait à progresser tant sur le plan professionnel que personnel. Physiquement, je ne dépasse toujours pas les 5 pieds 1 pouce, mais humainement, je l'ai largement dépassé. J'ai eu la chance de l'avoir pour me guider tout au long de ce processus. Enfin, je remercie mes amis et ma famille pour ce projet et pour tout ce que vous savez et pour lequel vous m'avez aidée. Easter Egg. Un merci particulier à Caroline Fink-Mercier pour tout ce qu'elle a fait en mon absence et un grand merci à mes collègues scientifiques qui ont rendu cette expérience si enrichissante.

Some of my scientific colleagues do not speak French, so to show respect, I want to express my gratitude by saying "Thank you" in addition to "Merci".

AVANT-PROPOS

Vers la fin des années 1990, les communautés cries de la côte est de la baie James ont alerté les autorités de la diminution de l'étendue et de la qualité des herbiers de zostères (*Zostera marina*). Cet événement pourrait avoir un impact inhérent sur la présence des bernaches (*Branta canadensis* et *Branta bernicla*) qui séjournent dans les herbiers de zostères lors de leur migration, notamment pour se nourrir. Ainsi, en plus de la détérioration écologique de leur territoire, les communautés cries subissent des conséquences culturelles et alimentaires, étant donné l'importance de la chasse traditionnelle comme moyen de se procurer de la viande de qualité.

Par ailleurs, jusqu'à tout récemment, relativement peu d'études scientifiques ont porté sur les propriétés physiques, chimiques et biologiques des eaux côtières de la baie James, malgré les impacts potentiels des aménagements hydroélectriques sur l'écosystème côtier amorcés dans les années 1970. Il y a donc un vide scientifique important qui ne peut être comblé par le savoir traditionnel des communautés cries. Ainsi, mon projet de maîtrise en océanographie chimique a été réalisé dans le cadre de l'Étude de l'océanographie des eaux côtières de l'est de la baie James (COast-JB) visant à mieux comprendre les facteurs environnementaux qui affectent l'écologie de la zostère marine.

L'important développement du vaste complexe hydroélectrique La Grande dans la région de la baie James affecte l'hydrologie des principales rivières à la suite de plusieurs dérivations qui ont fini par doubler le débit annuel de la Grande Rivière. La coexistence de rivières régulées et non régulées sur la côte est de la baie James offre une rare occasion d'évaluer l'effet des grands barrages hydroélectriques sur la qualité et la dynamique du carbone organique dissous chromophorique (CDOM) en aval dans les systèmes marins nordiques. Les objectifs de cette étude sont : 1) d'évaluer l'impact de la régulation du débit fluvial sur l'abondance et les caractéristiques chimiques du CDOM terrestre déversé dans l'est

de la baie James, 2) de caractériser la dynamique de mélange du CDOM et leur potentielle variabilité saisonnière et interannuelle dans la baie, et 3) d'étudier la possibilité d'utiliser la CDOM comme indicateur du carbone organique dissous dans l'est de la baie James. Les résultats de la présente étude comblent une lacune dans la connaissance de la matière organique dissoute dans la baie James et améliorent la compréhension du cycle biogéochimique de la matière organique et de l'optique de la colonne d'eau dans l'ensemble du système de la baie d'Hudson.

RÉSUMÉ

La matière organique dissoute chromophorique (CDOM) influence la répartition de la lumière et la biogéochimie dans les milieux aquatiques. Les eaux côtières directement impactées par le ruissellement fluvial reçoivent de grandes quantités de CDOM terrestre. La côte est de la baie James (EJB) abrite de nombreuses rivières, dont la plupart sont peu ou pas affectées par les activités humaines. La Grande Rivière (LGR) a cependant été fortement régulée pour construire un vaste complexe hydroélectrique de 1974 à 2013, comprenant de grands réservoirs et des canaux de dérivation. Les objectifs de ce projet sont 1) d'évaluer l'impact de la régulation du débit de la rivière sur l'abondance et les caractéristiques chimiques de la CDOM terrestre délivrée dans l'EJB, 2) de caractériser les dynamiques de mélange de la CDOM et leur variabilité saisonnière et interannuelle potentielle dans la baie, et 3) d'explorer la faisabilité d'utiliser la CDOM comme indicateur du carbone organique dissous (DOC) dans l'EJB. Pour atteindre ces objectifs, un plan d'échantillonnage pluriannuel (2018-2021) et multisaisonnier a été exécuté permettant la collecte des données de CDOM et du DOC ainsi que des données auxiliaires telles que la température de l'eau, la salinité et la composition isotopique de l'oxygène ($\delta^{18}O$-H_2O). L'eau douce déversée par la Grande Rivière largement régulée était constamment appauvrie en DOM par rapport aux rivières non régulées (URRs), avec un coefficient d'absorption de la CDOM à 440 nm ($a_{CDOM}(440)$) en moyenne 3,35 fois plus faible et un DOC 2,50 fois plus faible. En revanche, la pente spectrale d'absorption entre 275 et 295 nm ($S_{275\text{-}295}$, un proxy du poids moléculaire) et le coefficient d'absorption spécifique à 254 nm ($a_{CDOM}(254)$, un indicateur de l'aromaticité) de la CDOM des URR n'étaient que 10,6% inférieurs et 11,7% supérieurs à ceux de la CDOM de la LGR, respectivement. L'apport fluvial s'est avéré être la source dominante de CDOM dans la zone d'étude, avec peu d'influence de la formation ou de la fonte de la glace de mer. La répartition de la CDOM a révélé deux régimes distincts : la zone à faible teneur en CDOM influencée par la LGR au nord et la zone à forte teneur en CDOM influencée par les URRs au sud. Les deux zones ont montré de fortes relations conservatrices, mais distinctes entre $a_{CDOM}(440)$ et la salinité, convergeant vers un membre final commun (salinité ~25) avec peu de saisonnalité. Les données composites combinant les deux zones et toutes les saisons et années ont montré des relations non linéaires entre $S_{275\text{-}295}$, $a^*_{CDOM}(254)$ et $a_{CDOM}(440)$ et une corrélation linéaire simple robuste entre DOM et $a_{CDOM}(440)$. Cette étude suggère un fort impact de la régulation des rivières sur l'apport de CDOM dans l'EJB, révèle une faible variabilité saisonnière de la dynamique et des caractéristiques du mélange de la CDOM, et démontre la faisabilité de l'utilisation de la télédétection spatiale pour l'évaluation synoptique et en temps réel de la dynamique de la DOM et des cycles biogéochimiques associés dans l'EJB.

Mots clés : absorption de la CDOM; carbone organique dissous; régulation des rivières; côte est de la baie James

ABSTRACT

Chromophoric dissolved organic matter (CDOM) influences light distribution and biogeochemistry in aquatic environments. Coastal waters directly impacted by river runoff receive large amounts of terrestrial CDOM. The eastern James Bay (EJB) coast harbors numerous rivers, most of which are little or not affected by human activities. The La Grande River (LGR) has, however, been heavily regulated for building a vast hydroelectric powerplant complex between 1974 and 2013, including large reservoirs and diversion channels. The objectives of this project are to 1) assess the impact of river discharge regulation on the abundance and chemical characteristics of terrestrial CDOM delivered into the EJB, 2) characterize the mixing dynamics of CDOM and their potential seasonal and interannual variability in the bay, and 3) explore the feasibility of using CDOM as an indicator of dissolved organic carbon (DOC) in the EJB. To achieve these objectives, multi-year (2018-2021) and multi-season field surveys were conducted to collect CDOM and DOC data, along with ancillary data including water temperature, salinity, and oxygen isotopic composition ($\delta^{18}O$-H_2O). Freshwater discharged from the extensively regulated LGR was constantly depleted in DOM compared with the unregulated rivers (URRs), being on average 3.35 times lower in CDOM absorption coefficient at 440 nm ($a_{CDOM}(440)$) and 2.50 times lower in DOC. In contrast, the absorption spectral slope between 275 and 295 nm ($S_{275\text{-}295}$, a proxy of molecular weight) and the specific absorption coefficient at 254 nm ($a^*_{CDOM}(254)$, an indicator of aromaticity) of the URRs CDOM were only 10.6% lower and 11.7% higher than those of the LGR CDOM, respectively. Riverine input was found to be the dominant source of CDOM in the study area, with little influence from sea ice formation or melting. CDOM distribution fell into two distinct regimes: the LGR-influenced low-CDOM area in the north and the URRs-influenced high-CDOM area in the south. The two areas showed strong conservative but separate $a_{CDOM}(440)$–salinity relationships converging at a common marine endmember (salinity ~25) with little seasonality. The composite data combing both areas and all seasons and years exhibited non-linear relationships between $S_{275\text{-}295}$, $a^*_{CDOM}(254)$ and $a_{CDOM}(440)$ and a robust simple linear correlation of DOC to $a_{CDOM}(440)$. This study suggests a strong impact of river regulation on CDOM input into the EJB, reveals low seasonal variability of CDOM mixing dynamics and characteristics, and demonstrates the feasibility of using remote sensing from space for real-time and synoptical assessment of DOM dynamics and the associated biogeochemical cycles in the EJB.

Keywords: CDOM absorption; dissolved organic carbon; river regulation; eastern coast of James Bay

TABLE DES MATIÈRES

LISTE DES TABLEAUX

LISTE DES FIGURES

LISTE DES ABRÉVIATIONS, DES SIGLES ET DES ACRONYMES

$A(\lambda)$	Absorbance de la CDOM à la longueur d'onde λ (nm) / Absorbance of CDOM at wavelength λ (nm)
$a_{CDOM}(\lambda)$	Coefficient d'absorption népérien de la CDOM à la longueur d'onde λ (nm) / Napierian absorption coefficient of CDOM at wavelength λ (nm)
$a^*_{CDOM}(254)$	Coefficient d'absorption spécifique de la CDOM à 254 nm (c'est-à-dire $a_{CDOM}(254)$ normalisé par la concentration de DOC) / Specific absorption coefficient of CDOM at 254 nm (i.e., $a_{CDOM}(254)$ normalized by the concentration of DOC)
CDOM	Matière organique dissoute chromophorique / Chromophoric dissolved organic matter
DOC	Carbone organique dissous / Dissolved organic carbon
DOM	Matière organique dissoute / Dissolved organic matter
EJB	Est de la baie James / Eastern James Bay
E_2/E_3	Quotient E_2/E_3 (ratio de l'absorbance à 250 nm à celle à 365 nm) / E_2/E_3 quotient (ratio of absorbance at 250 nm to that at 365 nm)
l	Longueur du trajet de la cuvette spectrophotométrique (m) / Pathlength of the spectrophotometric cuvette (m)
LGR	La Grande Rivière / La Grande River
$S_{275-295}$	Pente spectral de l'absorption du CDOM entre 275 nm et 295 nm / Absorption spectral slope of CDOM between 275 nm and 295 nm

URRs Rivières non-régulées / Unregulated rivers

UV Ultraviolet

$\delta^{18}O$-H_2O La notation δ de la composition isotopique stable de l'oxygène dans l'eau (c'est-à-dire l'écart relatif du rapport isotopique de $^{18}O/^{16}O$ pour un échantillon par rapport à celui d'un standard.) / The δ notation of the stable isotopic composition of oxygen in water (i.e., the relative deviation of the isotopic ratio of $^{18}O/^{16}O$ for a sample from that for a standard)

LISTE DES SYMBOLES

α (alpha)	Facteur de fractionnement isotopique/ Isotopic fractionation factor
δ (delta)	Déviation de la composition isotopique par rapport à un standard / Isotopic composition deviation relative to a standard
λ (lambda)	Longueur d'onde / Wavelength

INTRODUCTION GÉNÉRALE

1. DYNAMIQUE DE LA MATIÈRE ORGANIQUE DISSOUTE CHROMOPHORIQUE (CDOM)

La matière organique dissoute (DOM, dissolved organic matter en anglais) est un mélange complexe et hétérogène de composés organiques dissous dans l'eau, que l'on trouve notamment dans les rivières qui la transportent vers les océans côtiers. La DOM des rivières provient de la dégradation de la faune et de la flore du bassin versant (c'est-à-dire DOM terrigène) et de la production ou de la transformation de matière par les organismes pélagiques et benthiques (c'est-à-dire DOM autochtone). La matière organique dissoute chromophorique (CDOM, chromophoric dissolved organic matter en anglais) est la fraction de la DOM qui absorbe le rayonnement ultraviolet (UV, 280-400 nm) et visible (400-700 nm) donnant la couleur brunâtre ou jaunâtre aux rivières qui en sont riches, par opposition aux eaux qui en sont pauvres, comme les eaux marines, qui sont plus transparentes.

1.1 Définition et indices optiques dérivés de la matière organique dissoute chromophorique (CDOM)

La concentration de la CDOM ne peut pas être mesurée directement. Au lieu de cela, le coefficient d'absorption de la CDOM est utilisé à titre d'indicateur de la concentration en CDOM, soit à des longueurs d'onde UV (ex., 350 nm) (Blough et Del Vecchio, 2002) ou à de courtes longueurs d'onde visible (ex., 412, 440, 442 nm) comme en télédétection (Siegel et al., 2002; Mabit et al., 2022). Plus la concentration est élevée, plus le coefficient d'absorption est élevé. Le coefficient d'absorption népérien (basé sur le logarithme naturel *e*) de la CDOM ($a_{\mathrm{CDOM}}(\lambda)$ en m^{-1}) est calculé selon l'équation 1 :

$$a_{CDOM}(\lambda) = \frac{2.303 \times A(\lambda)}{l} \qquad \text{Éq. 1}$$

où λ est la longueur d'onde en nm, A(λ) est la densité optique (ou l'absorbance) mesurée et *l* est la longueur du trajet de la cuvette en mètre.

De nombreuses études ont démontré qu'il est possible d'obtenir différents indicateurs en utilisant le spectre d'absorption. Le ratio entre le $a_{CDOM}(250)$ et le $a_{CDOM}(365)$, appelé le ratio E2/E3 (Éq. 2), est utilisé comme indice du poids moléculaire (De Haan et De Boer, 1987). E2/E3 diminue avec l'augmentation du poids moléculaire de la CDOM.

$$E2/E3 = \frac{a_{CDOM}(250)}{a_{CDOM}(365)} \qquad \text{Éq. 2}$$

Les pentes spectrales (*S*) sont aussi utilisées comme indices du poids moléculaire, mais elles sont aussi influencées par les processus de dégradation et par leur source (Twardowski *et al*., 2004; Helms *et al*., 2008; Granskog, 2012). *S* peut être obtenu en ajustant a_{CDOM} avec λ tel que présenté à l'équation 3 :

$$a_{CDOM}(\lambda) = a_{CDOM}(\lambda_0)e^{-S(\lambda-\lambda_0)} \qquad \text{Éq. 3}$$

où λ est la longueur d'onde en nm, λ_0 est la longueur d'onde de référence en nm et *S* est la pente en nm^{-1}. L'équation 3 décrit la décroissance exponentielle du $a_{CDOM}(\lambda)$ avec l'augmentation de la longueur d'onde et de la pente spectrale. La pente spectrale entre 275 et 295 nm ($S_{275\text{-}295}$) est probablement la pente spectrale la plus utilisée pour évaluer le poids moléculaire, la source et la nature de la dégradation de la CDOM (Helms *et al.*, 2008; Twardowski *et al*., 2004; Babin *et al.*, 2003; Fichot et Benner, 2012).

Le ratio des pentes (S_R), défini comme le ratio de $S_{275\text{-}295}$ à la pente spectrale entre 350 et 400 nm ($S_{350\text{-}400}$) (Éq. 4), est également corrélé avec le poids moléculaire (Helms *et al*., 2008).

$$S_R = \frac{S_{275-295}}{S_{350-400}} \qquad \text{Éq. 4}$$

Le coefficient d'absorption spécifique de la CDOM à 254 nm ($a^*_{CDOM}(254)$ en L (mg C)$^{-1}$ m^{-1}, specific absorption coefficient en anglais) est le $a_{CDOM}(254)$ normalisé par la

concentration en carbone organique dissous (DOC) en mg L^{-1}. C'est un indice qui témoigne de l'aromaticité de la CDOM (Weishaar *et al*., 2003). Plus le $a^*_{CDOM}(254)$ est élevé, plus l'aromaticité est élevée.

$$a^*_{CDOM}(254) = \frac{a_{CDOM}(254)}{DOC} \qquad \text{Éq. 5}$$

1.2 Les rôles de la CDOM dans les systèmes marins

La CDOM est l'absorbeur dominant du rayonnement UV et un absorbeur important du rayonnement visible dans l'océan (Nelson *et al.*, 1998; Nelson and Siegel, 2002; Siegel *et al.*, 2002), en particulier dans les eaux estuariennes et côtières. L'absorption du rayonnement UV-B (280-320 nm) atténue les effets nocifs des UV-B sur les organismes marins (Zepp, 2003; Häder *et al.*, 2011), tandis que l'absorption du rayonnement visible par la CDOM conflue avec la photosynthèse du phytoplancton pour le rayonnement photosynthétiquement actif (Mei *et al*., 2010). Par ailleurs, l'absorption du rayonnement visible par la CDOM affecte également avec la détection de la productivité primaire par télédétection (Bélanger *et al*., 2008), laquelle dépend de la réflectance de la lumière visible de la surface de la mer (Coble, 2007; Aurin *et al.*, 2013).

Dans la zone de mélange estuarienne, la CDOM des eaux fluviales peut être considérablement plus élevée que celle des eaux marines présentant de faibles concentrations. Dans le cas des estuaires où la dilution du CDOM est effectuée de manière quasi-conservative, la CDOM est un outil potentiel pour distinguer la contribution de ces deux sources d'eau (Aarup *et al.*, 1996; Granskog *et al*., 2007; Xie *et al*., 2012). L'existence des relations quantitatives entre le a_{CDOM} et le DOC dans les eaux côtières et estuariennes a fréquemment été observée. Puisque le a_{CDOM} peut être récupéré à distance (Bélanger *et al*., 2008; Aurin *et al*., 2013; Griffin *et al*., 2018), les concentrations de DOC peuvent être obtenues à partir de la télédétection spatiale. De plus, les coefficients d'absorption de la CDOM et/ou les indices optiques associés (Section 1.1) peuvent être utilisés pour retracer les circulations d'eau à l'échelle régionale ou mondiale (Nelson *et al.*, 2010). Plus récemment,

il a été constaté que $S_{275-295}$ était un bon indicateur de l'activité radiocarbone du DOC océanique (Song *et al*., 2023).

Enfin, l'absorption du rayonnement solaire par la CDOM entraine une série de réactions photochimiques ayant d'importantes implications optiques et biogéochimiques. Le rayonnement solaire, notamment sa bande UV, peut décomposer (c'est-à-dire oxyder) les chromophores de la CDOM, entraînant ainsi une perte d'absorbance (dit photoblanchiment) (Vodacek *et al*., 1997; Blough et Del Vecchio, 2002; Mopper et Kieber, 2002). Le photoblanchiment de la CDOM permet aux rayons UV solaires de pénétrer plus profondément dans l'eau amplifiant ainsi l'impact nocif des UV sur les organismes marins (Twardowski et Donaghay, 2002). La photo-oxydation de la CDOM produit également diverses espèces réactives de l'oxygène, telles que le radical hydroxyle, l'oxygène singulet et le peroxyde d'hydrogène (Mopper et Kieber, 2002; Altare et Vione, 2023), qui provoquent un stress oxydatif chez les organismes marins (Lesser, 2006) et modifient la spéciation de certains métaux traces (ex., le Fe et le Cu) et donc leur toxicité ou leur biodisponibilité (Blough et Zepp, 1995; Wells, 2002; Aiken *et al.*, 2011). La production de certains gaz à l'état de traces, tels que le CO_2, le CO, le CH_4 et les halogénures de méthyle, à partir de la photodégradation de la CDOM a des implications potentiellement importantes quant aux changements climatiques et/ou quant à la chimie atmosphérique (Erickson III *et al.*, 2014). La conversion du DOC en CO_2 lors de la photodégradation de la CDOM (c'est-à-dire photominéralisation) peut constituer un puits potentiellement important pour le DOC dans l'océan (Mopper *et al.*, 2015). En outre, la photo-oxydation modifie les caractéristiques de la CDOM. Lors de la dégradation photochimique de la CDOM terrigène, il y a une diminution de l'aromaticité et du poids moléculaire de la DOM restante (Lou et Xie, 2006; Helms *et al*., 2008; Stubbins *et al.*, 2008).

1.3 Comportement de mélange des CDOM terrigènes lors du transport vers la mer

Au cours du transport de l'eau des rivières vers la mer, la CDOM terrigène peut être éliminée de la colonne d'eau par floculation due aux changements de forces ioniques et du

pH (Gregor *et al.*, 1997; Asmala *et al.*, 2014) et par dégradation photochimique et microbienne (Section 1.2). D'autres processus, tels que la diffusion à partir des sédiments, l'apport d'eau souterraine et la production biologique in situ, peuvent ajouter de la CDOM à la colonne d'eau (Bauer et Bianchi, 2011). Le comportement de mélange (c'est-à-dire conservateur ou non-conservateur) de la CDOM terrigène dans les zones de transition eaux douces-vs-salées est généralement évalué à l'aide de diagrammes a_{CDOM}-vs-salinité en assumant que la salinité est conservatrice et qu'il n'existe que deux membres finaux (end-member en anglais), l'eau de mer et l'eau douce, qui se distingueraient par la salinité et la CDOM. Toutefois, dans les milieux côtiers à couverture de glace saisonnière, la formation et la fonte des glaces de mer créent des membres supplémentaires d'eau salée (rejet de saumure) et d'eau douce (fonte de la glace), ce qui rend l'utilisation de la salinité seule inadéquate pour évaluer le comportement de mélange de la CDOM terrigène (Östlund et Hut, 1984, Granskog *et al.*, 2015). Ainsi, des traceurs d'eau supplémentaires sont nécessaires pour identifier la provenance et le mélange des eaux.

La composition isotopique stable de l'oxygène dans l'eau s'est avérée être un outil utile pour discriminer les sources d'eau (Östlund et Hut, 1984; Granskog *et al.*, 2011). Chaque source d'eau est constituée d'un mélange caractéristique de l'isotope léger (^{16}O), naturellement plus abondant, et de l'isotope lourd (^{18}O). En raison des poids atomiques différents des deux isotopes, le fractionnement de ^{18}O et de ^{16}O se produit lors du transport ou de la transformation de l'eau dans le cycle hydrologique, entraînant un enrichissement ou un appauvrissement de l'isotope lourd (^{18}O). Le fractionnement isotopique respecte un équilibre cinétique et l'étendue du fractionnement peut être exprimée par le facteur de fractionnement (Éq. 6) (Rohling, 2013). La composition relative de ^{18}O et de ^{16}O est conventionnellement exprimée par les valeurs δ^{18}O-H_2O (Éq. 7) (Rohling, 2013).

$$\alpha_{A-B} = {}^{(18O/16O)_A}\Big/_{(18O/16O)_B} \qquad \text{Éq. 6}$$

$$\delta^{18}O = \left(\frac{(18O/16O)_{éch}}{(18O/16O)_{std}} - 1\right) \times 1000 \qquad \text{Éq. 7}$$

Dans ces équations, α est le facteur de fractionnement entre deux phases A et B (gaz et/ou liquide et/ou solide) et $\delta^{18}O\text{-}H_2O$ (‰) est l'écart du rapport $^{18}O/^{16}O$ d'un échantillon (éch) par rapport à celui d'un standard (std) VSMOW (Vienna Standard Mean Ocean Water ou Eau Océanique Moyenne Standard de Vienne en français).

Les eaux de ruissellement sont généralement discernables par leur salinité presque nulle et un $\delta^{18}O\text{-}H_2O$ négatif donc appauvrit en ^{18}O. L'appauvrissement en ^{18}O dans les eaux de ruissellement provient de l'élimination préférentielle de ^{18}O (par rapport à ^{16}O) de la phase gazeuse (vapeur) lors de l'évaporation de l'eau (Rohling, 2013). Les eaux marines ont une salinité élevée et un $\delta^{18}O\text{-}H_2O$ près de 0‰ mais qui peut être légèrement négatif dans les régions à haute latitude en réponse au mélange avec les précipitations (LeGrande et Schmidt, 2006; Roberts *et al*., 2011). Les eaux issues de la fonte des glaces de mer sont faiblement salées, suite au rejet des sels lors de la formation de la glace, avec un $\delta^{18}O\text{-}H_2O$ enrichi par rapport à l'eau de mer puisque le fractionnement est moins important que le rejet des saumures (Rohling, 2013).

2. LE CYCLE HYDROLOGIQUE

Le système de la baie d'Hudson inclut le bassin de Foxe, le détroit d'Hudson, la baie d'Hudson et la baie James (Figure 1). Le contenu en eau douce de cette vaste mer intérieure dépend principalement du ruissellement des bassins versants, des précipitations directes et de la fonte de la glace de mer au printemps (El-Sabh et Koutitonski, 1977; Prinsenberg, 1988; Déry *et al.*, 2005; Granskog *et al.*, 2011; Figure 2).

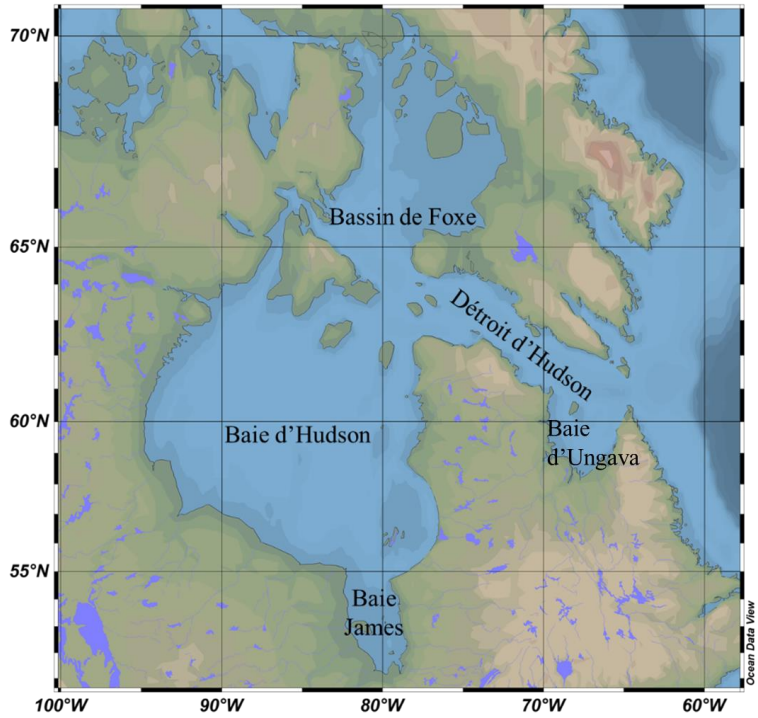

Figure 1. Carte du système de la baie d'Hudson.

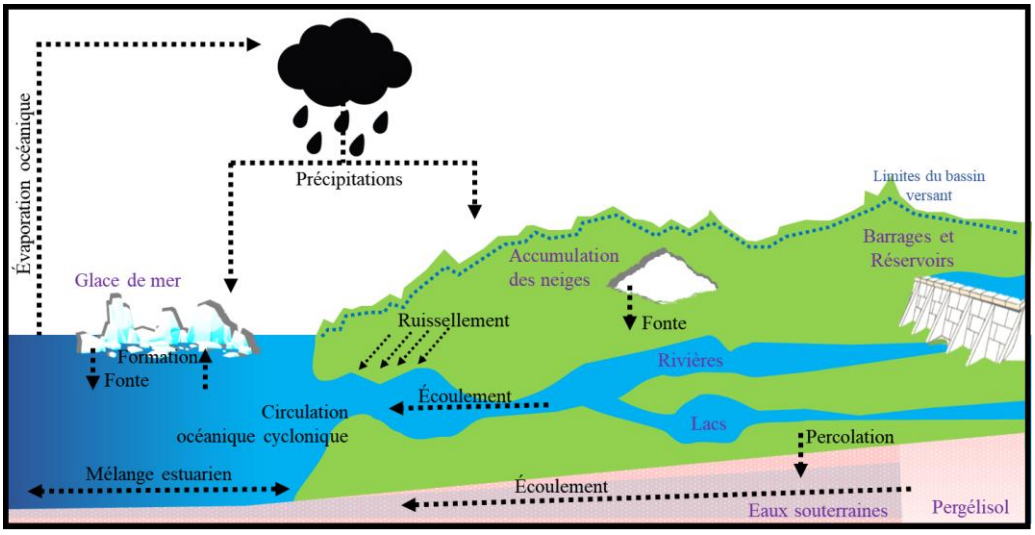

Figure 2. Schéma du cycle hydrologique illustrant l'ensemble des transferts d'eau (liquide, solide ou gazeuse) entre les réservoirs d'eau de la Terre (océans, atmosphère, lacs, rivières, nappes phréatiques et glace de mer). Le "moteur" de ce cycle est l'énergie solaire qui, en favorisant l'évaporation de l'eau, entraîne tous les autres échanges.

2.1 Changement anthropique : le complexe hydroélectrique La Grande

Avec la signature de la Convention de la baie James et du Nord québécois en 1975, le gouvernement du Québec a pu lancer officiellement les projets de développement du réseau hydroélectrique de la baie James (Figure 3). Le complexe hydroélectrique La Grande a été construit en trois phases, respectivement de 1973 à 1985, de 1987 à 1996 et de 2002 à 2012. Aujourd'hui, le complexe comprend 11 centrales hydroélectriques : La Grande-1 (1995), Robert-Bourassa (1981), La Grande-2-A (1992), La Grande-3 (1984), La Grande-4 (1986), Laforge-1 (1994), Laforge-2 (1996), Brisay (1993), Eastmain-1 (2006), Eastmain-1-A (2012) et Sarcelle (2013) (Lalumière et Lemieux, 2002; Schetagne *et al*., 2002). Les modifications apportées au territoire dans le cadre de ce projet, dont le détournement complet ou partiel de nombreuses rivières (Caniapiscau, Opinaca, Koksoak, Eastmain, Vincelotte, Sakami, Petite rivière Opinaca et Rupert) vers la Grande Rivière, l'augmentation ou la diminution du débit saisonnier des rivières et la construction de réservoirs, ont entraîné des changements importants dans les cycles biogéochimiques (Schetagne *et al.*, 2002). D'ailleurs, certaines de ces rivières se jetaient auparavant dans la baie d'Hudson et la baie d'Ungava, alors que d'autres se déversaient déjà dans la baie James. Ces changements ont doublé le potentiel énergétique de la Grande Rivière, dont le débit moyen annuel est passé de 1 700 $m^3\ s^{-1}$ à 3 400 $m^3\ s^{-1}$ (Schetagne *et al.*, 2002; de Melo *et al.*, 2022).

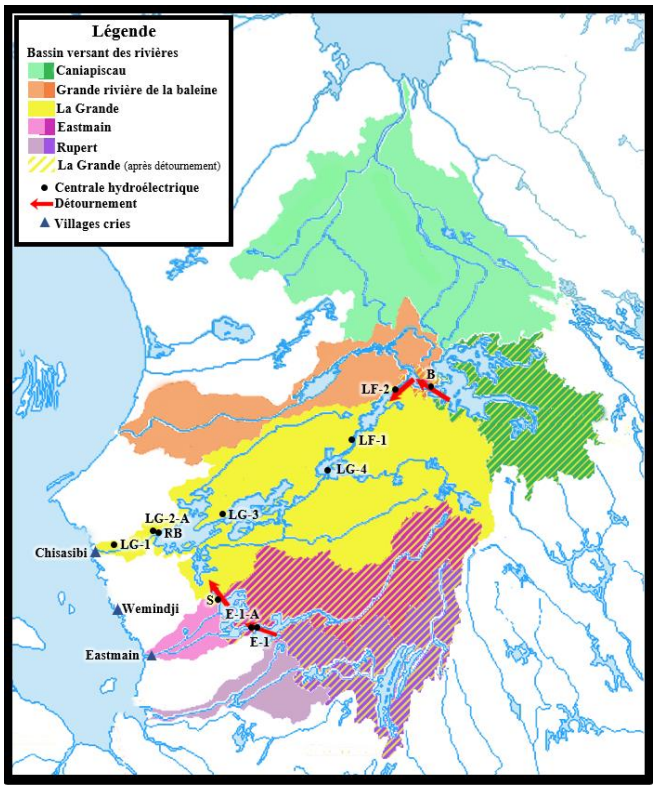

Figure 3. Carte de l'aménagement et du bassin versant du complexe hydroélectrique de la Grande Rivière.

2.2 Le système de la baie d'Hudson

Les bassins de drainage des baies d'Ungava, d'Hudson et James couvrent approximativement $3{,}7 \times 10^6$ km^2, soit le tiers de la superficie du Canada. Avec un débit annuel moyen de 272 km^3, les rivières de la baie James contribuent à 38,0% du débit total des 42 rivières se jetant dans ces baies, et ce, même si le bassin versant de la baie James ne couvre seulement que 18,5% du territoire total (Déry *et al.*, 2005). Dans la baie James, le rendement annuel du ruissellement serait plus élevé sur la côte est (186.96 km^3 an^{-1}) que sur la côte ouest (84.53 km an^{-1}; Déry *et al.*, 2005). À l'exception de la Grande Rivière où le débit est maximal durant l'hiver (environ 11%) et minimal en mai (environ 7%), le débit des rivières à l'est de la baie James serait minimal à l'hiver ($\leq$ 4%) et maximal de la fin mai au début juin (environ 16%) pendant la crue printanière avec un décalage temporel entre le sud

et le nord (El-Sabh et Koutitonski, 1977; Prinsenberg, 1986; Déry et *al*, 2005; Hernández-Henríquez *et al.*, 2010). Par contre, le débit de la Grande Rivière est plus important en hiver afin de pouvoir répondre à l'augmentation de la demande en électricité (Jia *et al.*, 2019). À partir de novembre, une couche de glace de mer d'une épaisseur maximale de 1 m se forme sur toute la surface de la baie James (Prinsenberg, 1988; Saucier et Dionne, 1998). Vers la fin mai ou début juin, la glace commence à se briser. Prinsenberg (1988) estime qu'environ le tiers de l'eau douce apportée dans la baie James provient de la fonte des glaces marines et que le reste provient du ruissellement.

De plus, comparativement à la baie d'Hudson, où le rapport évaporation/précipitation est élevé (5:3), la baie James se distingue par son caractère moins océanique. En effet, son taux de précipitations directes s'équilibre annuellement avec son taux d'évaporation, même si les précipitations directes représentaient moins de 10% des précipitations vers le bassin versant (Prinsenberg, 1980).

Quant à l'eau marine, elle provient de la baie d'Hudson et s'écoule à la surface dans la baie James grâce à la circulation cyclonique issue du forçage par le vent (lorsque la vitesse du vent est supérieure à 10 nœuds et lorsque la baie n'est pas couverte de glace de mer) et/ou par le forçage gravitationnel (El-Sabh et Koutitonsky, 1977). L'eau marine de la baie d'Hudson se mélange, entre autres, par cisaillement, aux eaux douces des rivières du sud-ouest de la baie d'Hudson et des rivières de la côte ouest de la baie James, avant de se diriger vers le nord en longeant la côte est de la baie James. L'eau marine peut également entrer dans la baie James en profondeur sur toute la largeur de la connexion avec la baie d'Hudson (El-Sabh et Koutitonsky, 1977).

Avec l'apport important d'eau douce des rivières, la baie James, et en particulier sa côte est, reçoit sept fois plus d'eau douce que sa côte ouest (Meilleur et al., 2023). En conséquence, la baie James accumule des quantités significatives de matière organique dissoute, estimées à 698 µmol L-1 par Mundy *et al*. (2010). La matière organique terrigène serait d'ailleurs la source principale de matière organique dans le système de la baie James (Guéguen *et al*., 2011). Le cycle hydrologique est intimement relié au cycle du carbone et il a un rôle

important quant à la répartition et aux propriétés de la DOM dans la baie James. Lors de la formation de la glace de mer en hiver, la saumure et la DOM de la glace sont rejetées dans la colonne d'eau (Müller *et al.*, 2013). Cette eau plus dense coule et entraîne la DOM dans les eaux plus profondes. De plus, sous la couverture de glace, l'exposition aux rayons solaires est réduite diminuant la transformation photochimique de la DOM. En revanche, au printemps, l'eau issue de la fonte de la glace de mer dilue la DOM des eaux de surface.

2.3 Les changements climatiques

Le Groupe d'experts intergouvernemental sur l'évolution du climat (GIEC) a constaté une forte augmentation des températures de l'air en Arctique qui serait plus du double de la moyenne mondiale (Jia *et al*., 2019). Les changements dans l'environnement (température atmosphérique, épaisseur, l'étendue et durée de la couverture de glace hivernale, dégel du pergélisol, et précipitations) affectent le cycle hydrologique (Pohl *et al*., 2007). L'ampleur du changement climatique est d'autant plus importante dans le nord du Canada, notamment dans la zone subarctique, où les changements sont beaucoup plus rapides que dans le reste du monde (Kaufman *et al*., 2009) qu'il s'agisse de l'atmosphère, de l'hydrosphère, de la cryosphère ou de la biosphère.

Dans la région de la baie d'Hudson (incluant la baie James), la température des eaux de surface a augmenté entre 1992 et 2009, et cette augmentation est plus marquée durant l'été qu'en hiver (Galbraith et Larouche, 2011). À la fin des années 1990s, des anomalies positives de température ont été observées pendant quatre années consécutives, soit entre 1998 et 2001 (Galbraith et Larouche, 2011). L'année 1998 a été marquée par un évènement d'oscillation australe El Niño (ENSO) particulièrement intense au Canada, qui a eu plusieurs répercussions comme la tempête de verglas qu'a connue le Québec en janvier 1998 (Barsugli *et al*., 1999). Cet évènement s'est distingué par sa durée, son étendue spatiale et la quantité de glace accumulée et est associé à un front chaud. Autrement, plusieurs feux de forêts ont été observés dans cette région. Les températures atmosphériques élevées, combinées à de faibles précipitations, ont été identifiées comme l'une des conditions météorologiques

extrêmes aggravant l'ampleur des feux de forêt dans cette région (Erni *et al*., 2016). C'est le cas de l'incendie d'Eastmain en 2013, l'un des cinq incendies majeurs de la région (1847, 1922, 1941, 1989 et 2013) qui a été provoquée par la foudre et s'est propagé sur 5 830 km^2 en 5 semaines (Erni *et al*., 2016). Il a persisté grâce aux températures de 26 à 28 °C le midi avec des vents moyens de 33 km/h et des précipitations 34.6 mm contre une moyenne mensuelle de 65.3 mm pour le mois de Juin. Ces événements peuvent avoir un impact sur le cycle du carbone en libérant du CO_2 dans l'atmosphère et de la matière organique terrigènes qui est exportée par ruissellement vers les rivières et la baie James.

Dans le système de la baie d'Hudson, la baie James se distingue par sa température moyenne de surface la plus élevée, atteignant 10,20 °C (Galbraith et Larouche, 2011). Cette caractéristique est étroitement liée au moment du dégel de la couverture de glace, avec une variation de la régression linéaire représentant 58 % de cette corrélation, et est positivement corrélée (R^2 = 0,80) aux températures atmosphériques suivant le dégel (Galbraith et Larouche, 2011). De plus, le changement climatique entraînerait un retard dans la formation des glaces de mer et une réduction de 5 à 50% de l'épaisseur de la glace dans tout le système de la baie d'Hudson (Senneville et St-Onge Drouin, 2013; Taha *et al*., 2019).

Il est difficile de distinguer l'impact du changement climatique de ceux associés aux modifications anthropiques quant aux variabilités journalières, interannuelles et interdécennales du débit des rivières (Déry *et al*., 2016). Toutefois, la variabilité accrue des apports en eau douce des rivières observées entre 2004 et 2013 semble être associée au climat, et ce, pour l'ensemble du système de la baie d'Hudson.

Thibault et Payette (2009) ont observé en Jamésie (Québec) que la limite longitudinale du pergélisol était autour de 53°N en 2004 et 2005, mais qu'entre ces deux années le pergélisol s'est fortement dégradé et qu'il ne serait plus présent dans un avenir rapproché. Plusieurs études suggèrent d'ailleurs que l'étendue du pergélisol était auparavant plus grande, sa limite atteignant des latitudes plus au sud (Vincent, 1977; Dionne, 1978; Thibault et Payette, 2009). La libération de la matière organique séquestrée sous la surface terrestre par

le dégel du pergélisol est susceptible d'avoir influencé la composition chimique et les propriétés optiques des rivières qui se jettent dans la baie James (Wologo *et al*., 2021).

3. OBJECTIFS

L'important développement hydroélectrique de la région de la baie James affecte l'hydrologie des principales rivières à la suite de plusieurs dérivations qui ont fini par doubler le débit annuel de la Grande Rivière (Déry *et al*., 2016). La coexistence de rivières régulées et non régulées sur la côte est de la baie James offre une rare occasion d'évaluer l'effet des grands barrages hydroélectriques sur la qualité et la dynamique de la matière organique dissoute chromophorique (CDOM) en aval dans les systèmes marins nordiques. Les objectifs de cette étude sont les suivants 1) d'évaluer l'impact de la régulation du débit des rivières sur l'abondance et les caractéristiques chimiques de la CDOM terrestre déversée dans l'est de la baie James, 2) de caractériser la dynamique de mélange de la CDOM et sa potentielle variabilité saisonnière et interannuelle dans la baie, et 3) d'étudier la possibilité d'utiliser la CDOM comme indicateur du carbone organique dissous dans l'est de la baie James.

CHAPITRE 1
RIVIÈRES RÉGULÉES ET NON-REGULÉES : L'IMPACT SUR LA DYNAMIQUE DE LA CDOM DANS L'EST DE LA BAIE JAMES

1.1 RÉSUMÉ EN FRANÇAIS DE L'ARTICLE

La côte orientale de la baie James (EJB) abrite de nombreuses rivières, mais un manque de connaissances sur la matière organique dissoute (DOM) dans les eaux côtières en aval de la limite riveraine subsiste. Nous rapportons ici une étude de terrain de quatre ans (2018-2021) sur plusieurs saisons sur le comportement de mélange et les caractéristiques de la DOM chromophorique (CDOM) dans l'EJB littorale. L'eau douce provenant de la Grande Rivière (LGR), largement régulée pour la production d'hydroélectricité, était constamment appauvrie en DOM par rapport aux rivières non régulées (URRs); le coefficient d'absorption de la CDOM à 440 nm ($a_{CDOM}(440)$) et le carbone organique dissous (DOC) étant respectivement 3,35 et 2,50 fois plus faible en moyenne. En revanche, la pente spectrale d'absorption entre 275 et 295 nm ($S_{275-295}$, un proxy du poids moléculaire) et le coefficient d'absorption spécifique à 254 nm ($a^*_{CDOM}(254)$, un indicateur d'aromaticité) de la CDOM des URRs n'étaient que 10,6% inférieurs et 11,7% supérieurs à ceux de la CDOM de LGR, respectivement. L'apport fluvial s'est révélé être la source dominante de la CDOM dans la zone d'étude, avec peu d'influence de la formation ou de la fonte des glaces de mer. Les données de la CDOM se répartissent en deux régimes distincts, soit la zone à faible CDOM influencée par LGR au nord et la zone à CDOM élevée influencée par les URRs au sud. Les deux zones ont montré de fortes relations conservatives, mais distinctes entre le $a_{CDOM}(440)$ et la salinité, convergeant vers un membre final marin commun (salinité ~ 25) et avec peu de différences saisonnières. Les données composites combinant les deux zones et toutes les saisons et années dénotaient des relations non linéaires entre $S_{275-295}$, $a^*_{CDOM}(254)$ et $a_{CDOM}(440)$ et une forte corrélation linéaire entre le DOC et $a_{CDOM}(440)$. Cette étude suggère

un fort impact de la régulation des rivières sur l'apport de la CDOM dans l'EJB. Elle révèle une faible variabilité saisonnière de la dynamique de mélange et des caractéristiques de la CDOM, et démontre la faisabilité de l'utilisation de la télédétection depuis l'espace pour l'évaluation synoptique et en temps réel de la dynamique du DOM et des cycles biogéochimiques associés dans l'EJB.

Cet article, intitulé « *Regulated vs. unregulated rivers: impacts on CDOM dynamics in the eastern James Bay* » (https://doi.org/10.1016/j.marchem.2023.104309), a été évalué par les pairs et accepté pour publication dans sa version finale en 2023 par les éditeurs de la revue *Marine Chemistry*. Comme mentionnée à la section « Author Contribution » (Section 1.7.3), ma contribution en tant que premier auteur inclus la conceptualisation, l'échantillonnage, l'analyse et le traitement des données, la rédaction du premier jet de cet article et la correction du manuscrit final et avec l'aide et sous la supervision de H. Xie et M. Gosselin et sous la supervision de V. Galindo pour les campagnes d'échantillonnage. En plus de superviser la dernière campagne d'échantillonnage, d'en analyser et traiter les données, C. Fink-Mercier a rédigé le deuxième jet avec l'original comme basse en intégrant des données manquantes (automne 2018, printemps 2019, hiver 2020 et été 2021) et ce également en collaboration avec H. Xie. Étant responsable du programme de recherche avec M. Gosselin, U. Neumeier a participé à la conceptualisation du programme de recherche dans son ensemble. Tous les auteurs ont commenté le manuscrit.

En plus de l'article, le contenu de cet article a été présenté à plusieurs occasions lors de congres, symposiums et autres activités de vulgarisation.

Évrard, A., Xie, H., Gosselin, M., Bélanger, S., Galindo, V. et Neumeier, U. (2018). Spatial distribution of freshwater sources covering eelgrass beds along the east coast of James Bay. Réunion scientifique annuelle de Québec-Océan, Rivière-du-Loup, Québec, Canada, 5-6 novembre (Affiche).

Évrard, A., Xie, H., Gosselin, M., Bélanger, S., Galindo, V. et Neumeier, U. (2019). Eastern James Bay water column chemistry. Yaayimutitaau Shikaapaashkwh Symposium, Chisasibi, Québec, Canada, 29-31 janvier (Affiche).

Évrard, A., Xie, H., Gosselin, M., Bélanger, S., Galindo, V. et Neumeier, U. (2019). Freshwater sources and characteristics of chromophoric dissolved organic matter (CDOM) along the coast of eastern James Bay. ArcticNet Annual Scientific Meeting, Halifax, Nouvelle-Écosse, Canada, 1-5 décembre (Présentation orale).

Évrard, A. et Xie, H. (2020). Répartition spatio-temporelle des sources en eau douce dans l'est de la baie James déduite de la salinité et de la matière organique dissoute chromophorique (CDOM). Réunion scientifique annuelle de Québec-Océan, Beaupré, Québec, Canada, 9-11 mars (Présentation orale).

1.2 REGULATED VS. UNREGULATED RIVERS: IMPACTS ON CDOM DYNAMICS IN THE EASTERN JAMES BAY

1.3 ABSTRACT

The eastern James Bay (EJB) coast harbors numerous rivers, but there is a dearth of knowledge concerning dissolved organic matter (DOM) in the downstream coastal water. Here we report a four-year (2018–2021) and multi-seasons field study on the mixing behavior and characteristics of the chromophoric DOM (CDOM) in the nearshore EJB. Freshwater discharged from the extensively regulated La Grande River (LGR) was constantly depleted in DOM compared with the unregulated rivers (URRs), being on average 3.35 times lower in CDOM absorption coefficient at 440 nm ($a_{CDOM}(440)$) and 2.50 times lower in dissolved organic carbon (DOC). In contrast, the absorption spectral slope between 275 and 295 nm ($S_{275\text{-}295}$, a proxy of molecular weight) and the specific absorption coefficient at 254 nm ($a^*_{CDOM}(254)$, an indicator of aromaticity) of the URRs CDOM were only 10.6% lower and 11.7% higher than those of the LGR CDOM, respectively. Riverine input was found to be the dominant source of CDOM in the study area, with little influence from sea ice formation or melting. CDOM distribution fell into two distinct regimes: the LGR-influenced low-CDOM area in the north and the URRs-influenced high-CDOM area in the south. The two areas showed strong conservative but separate $a_{CDOM}(440)$–salinity relationships converging at a common marine endmember (salinity ~25) with little seasonality. The composite data combing both areas and all seasons and years exhibited non-linear relationships between $S_{275\text{-}295}$, $a^*_{CDOM}(254)$ and $a_{CDOM}(440)$ and a robust simple linear correlation of DOC to $a_{CDOM}(440)$. This study suggests a strong impact of river regulation on CDOM input into the EJB, reveals low seasonal variability of CDOM mixing dynamics and characteristics, and demonstrates the feasibility of using remote sensing from space for real-time and synoptical assessment of DOM dynamics and the associated biogeochemical cycles in the EJB.

1.4 INTRODUCTION

Pan-arctic estuaries receive large amounts of dissolved organic carbon (DOC) from rivers (McClelland *et al*., 2012). In highly riverine systems, chromophoric dissolved organic matter (CDOM) of terrestrial origin has been shown to be the major contributor to the dissolved organic matter (DOM) pool (Guéguen *et al*., 2011), making it a proxy for DOC concentration in some regions (e.g., Fichot and Benner, 2011; Stedmon *et al*., 2011; Asmala *et al*., 2012). The input of CDOM in these estuaries has important implications for coastal biogeochemistry as it absorbs solar ultraviolet (UV) and visible radiation, thereby reducing light penetration into the water column (Bricaud *et al*., 1981), mitigating UV damaging to aquatic organisms (Zepp, 2003), competing with photosynthesizers for visible radiation (Mei *et al*., 2010), and interfering with remote sensing of marine primary productivity (Bélanger *et al*., 2008). While CDOM distributions have been relatively well described in several northern marine environments (Massicotte *et al*., 2017), in part because CDOM can be retrieved remotely (Bélanger *et al*., 2008; Aurin *et al*., 2013; Griffin *et al*., 2018), the projected increases in freshwater discharge (Guay *et al*., 2015), permafrost thaw, and coastal development in northern regions are suspected to result in changes in CDOM input (Xenopoulos *et al*., 2021; Blanchet *et al*., 2022), with impacts on coastal biogeochemistry.

The fate of CDOM in aquatic systems is dictated by loading and loss processes. The abundance and composition of CDOM that enters the estuary depend on the landscape characteristics of the watershed where it is loaded, with wetlands and high discharge rivers generally loading larger amounts of aromatic CDOM (Spencer *et al*., 2013; Massicotte *et al*., 2017). During its freshwater-saltwater transition, CDOM is gradually transformed and lost due to various physical (e.g., mixing and flocculation) (Asmala *et al*., 2014), biological (e.g., microbial degradation or production), and chemical (e.g., photodegradation) processes (Logozzo *et al*., 2021; Kragh *et al*., 2022). The processing of CDOM along the water continuum not only changes the abundance but also alters the quality of CDOM, notably its molecular weight and aromaticity (Helms *et al*., 2008; Massicotte *et al*., 2017).

A variety of tools has been used to describe both the quantity and the quality of CDOM in aquatic environments. Absorption coefficients (a_{CDOM}) at UV and short visible wavelengths are widely used to characterize the quantity of CDOM, while the absorption spectral slope between 275 and 295 nm ($S_{275-295}$) and the specific absorption coefficient at 254 nm ($a^*_{CDOM}(254)$) are used as proxies of its molecular weight and aromaticity, respectively (Weishaar *et al*., 2003; Helms *et al*., 2008). Changes in these proxies reflect the degree of mixing and/or processing of CDOM along the water continuum. Linear relationships between a_{CDOM} and salinity have been found in many estuarine and coastal water bodies (Granskog *et al*., 2007; Guéguen *et al*., 2011; Markager *et al*., 2011; Asmala *et al*., 2016), reflecting the conservative mixing of CDOM in river water and CDOM in seawater. On the other hand, deviation from the linear mixing curve indicates net addition or removal of CDOM. These conservative or non-conservative behaviors may change seasonally, depending on the seasonality of CDOM sources and sinks and estuarine hydrodynamics (Markager *et al*., 2011; Asmala *et al*., 2016; Li *et al*., 2019).

James Bay is the most river-influenced water body of the Hudson Bay system (Déry *et al*., 2005) and is likely a major contributor to its CDOM budget (Meilleur *et al*., 2023). James Bay contributes 38.0% of the total annual freshwater input to Hudson Bay, with the majority (26.3%) from the east coast of James Bay. Export of riverine DOM into the eastern James Bay has recently been shown to vary with watershed landscape composition (de Melo *et al*., 2022), but little is known about its fate in the James Bay marine system. In fact, several studies have been conducted in Hudson Bay to elucidate the distributions, sources, optical characteristics, and photoreactivity of CDOM (Granskog *et al*., 2007, 2009; Guéguen *et al*., 2011, 2016; Meilleur *et al*., 2023), but these studies did not cover much of James Bay. Past surveys in Hudson Bay are also limited for addressing potential seasonal and interannual variability of CDOM associated with temporal fluctuation of river discharge (Meilleur *et al*., 2023). In fact, there is an overrepresentation of summer months compared to other seasons in the CDOM literature (Massicotte *et al*., 2017). Furthermore, the extensive hydroelectric development in the region affects the hydrology of major rivers following several diversions ultimately doubling the annual discharge of the La Grande River (LGR) (Déry *et al*., 2016).

The coexistence of both regulated (i.e., the LGR) and unregulated rivers (URRs) on the east coast of James Bay provides a rare opportunity to assess the effect of large hydroelectric river dams on the downstream CDOM quality and dynamics in northern marine systems.

The objectives of this study are to 1) assess the impact of riverine discharge regulation on the abundance and chemical characters of terrestrial CDOM delivered into the eastern James Bay, 2) characterize the mixing dynamics of CDOM and their potential seasonal and interannual variability in the bay, and 3) explore the feasibility of using CDOM as an indicator of DOC in the eastern James Bay. Results from the present study fill a knowledge gap of DOM in James Bay and improve the understanding of biogeochemical cycling of DOM and water column optics in the Hudson Bay system as a whole.

1.5 METHODS

1.5.1 Study area

Located on the southern end of the Hudson Bay system, James Bay covers an area of 68 300 km^2 and has an average depth of 28 m (Figure 4). Surface circulations are generally cyclonic and are characterized by a narrow, strong northward outflow along the eastern side of the bay and a broad, weak southward inflow from Hudson Bay along the western side (El-Sabh and Koutitonsky, 1977; Prinsenberg, 1986). Sea ice in James Bay generally begins to form in December and reaches a maximum depth of ~1 m during winter. In May, sea ice starts to melt and its contribution to the freshwater budget of James Bay can overtake river runoff (Prinsenberg, 1988; Taha *et al*. 2019). The cyclonic circulation, spatiotemporally asymmetric river discharge, and sea ice formation and melting are among the major contributors to large spatial and seasonal variations of James Bay's surface water temperature and salinity and water column stratification (Prinsenberg, 1986).

Numerous rivers flow into the eastern James Bay (Figure 4) at freshwater discharge rate of about 227 $km^3\ yr^{-1}$ (de Melo *et al*., 2022). The successive partial diversions of the Caniapiscau River, Grande rivière de la Baleine, Eastmain River, and Rupert River from

1980 to 2009 more than doubled the annual freshwater discharge of the LGR. In counterpart, the flows of some of these rivers have severely been reduced, with the Eastmain and Caniapiscau rivers only discharging 10% and 60% of their original flows, respectively (Roy and Messier, 1989; Déry *et al*., 2005). Currently, the LGR is the largest river of the Hudson Bay system and supplies ~14% of the total annual river discharge into Hudson Bay. While the natural rivers in the region follow a typical northern river hydrograph with peak discharge in spring and base flow in winter, the seasonal discharge pattern of the LGR is inverted and flattened due to regulation for hydroelectricity production, with peak flow occurring during winter when electricity demand is highest (Déry *et al*., 2016). The eastern coast of James Bay, also called Eeyou Istchee, is home to the Cree communities of Waskaganish, Eastmain, Wemindji and Chisasibi. The land is divided into 27 coastal traplines, which serve as the delimitation of hunting grounds for Cree families (Figure 5).

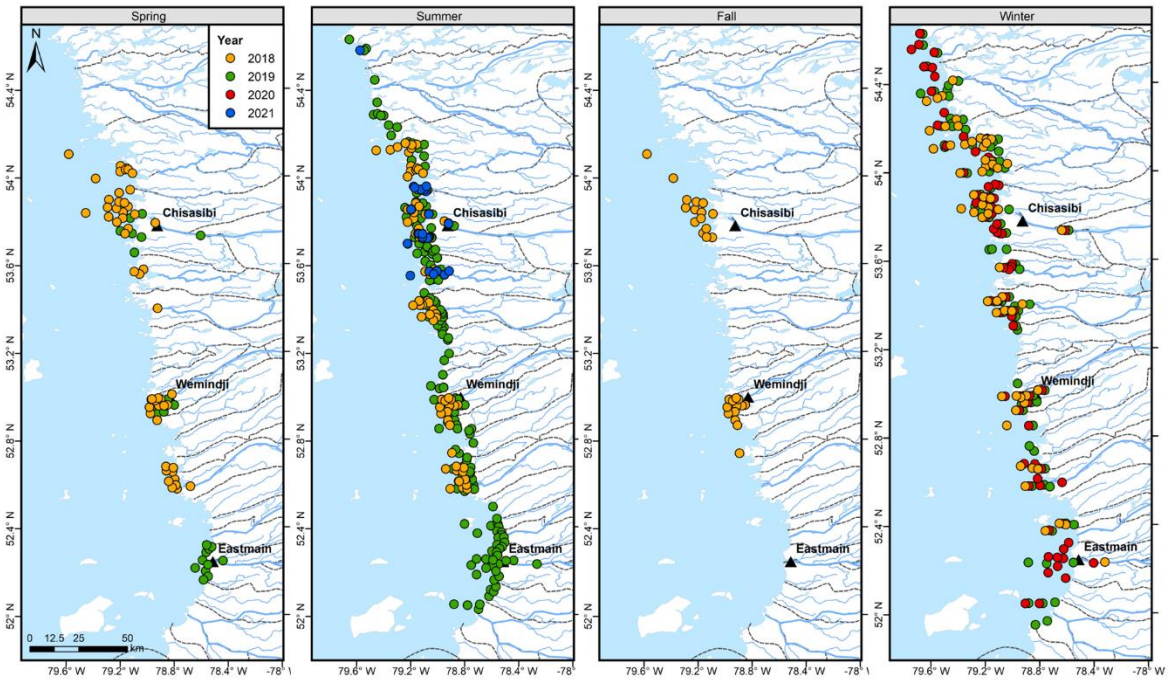

Figure 5. Maps of sampling stations from spring (left) to winter (right). Points are slightly offset to show all sampling points. Dashed lines show trapline locations.

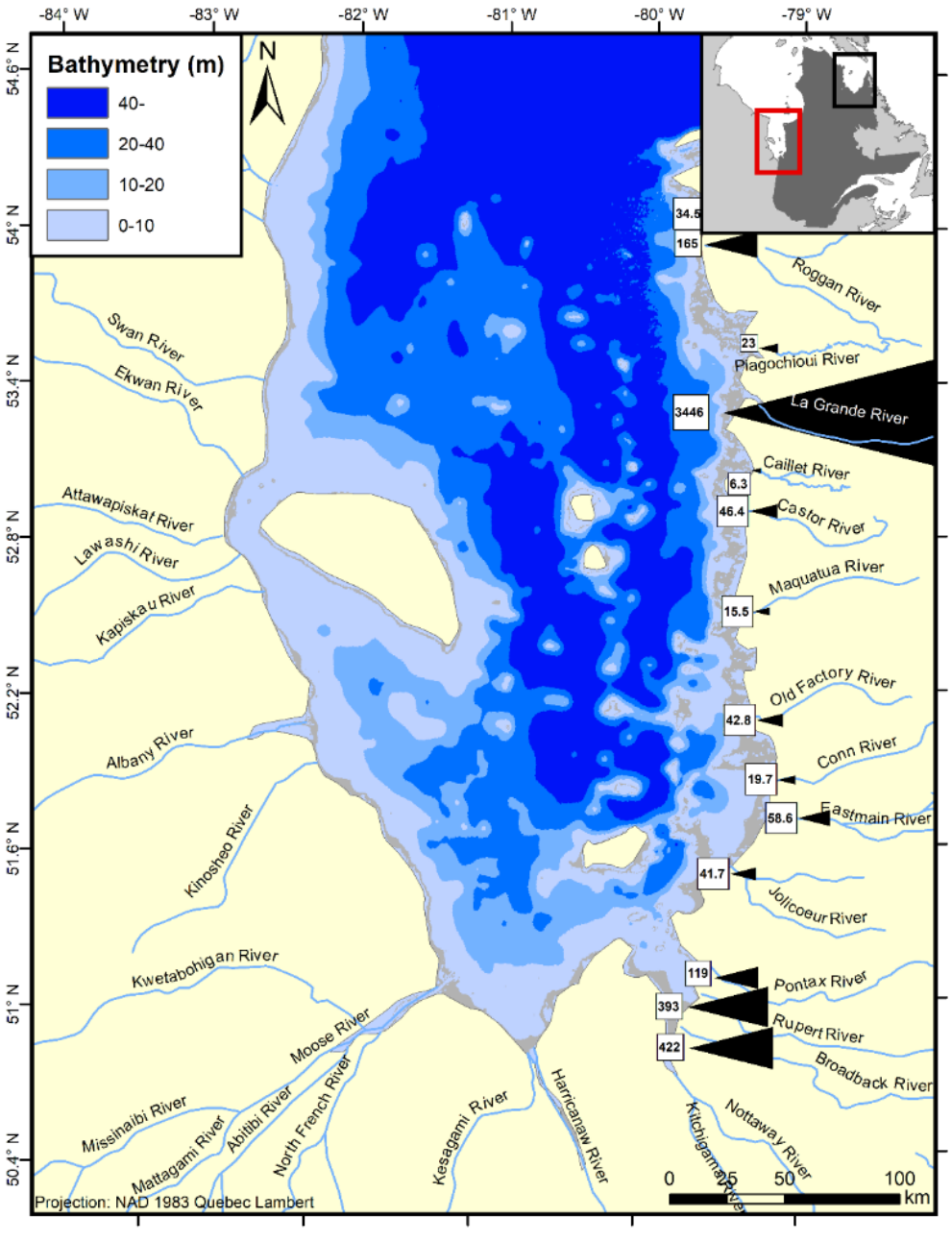

Figure 4. James Bay region and its major rivers. The triangles illustrate the mean annual discharges ($m^3\ s^{-1}$) of the eastern James Bay rivers measured or modelled by de Melo et al. (2022). The insert shows the location of James Bay (red rectangle) and Ungava Bay (black rectangle).

1.5.2 Sampling

Water sampling was conducted as part of the Coastal Oceanography of Eastern James Bay (COast-JB) project aiming to better understand the environmental factors that affect the eelgrass (*Zostera marina*) ecology in the eastern James Bay. Sampling stations were located in nearshore waters (< 40 m deep) between 52.2°N and 54.5°N (Figure 5) and visited in the summers of 2018, 2019, and 2021, the fall of 2018, the winters of 2018, 2019, and 2020, and the springs of 2018 and 2019 (Table 1). Coordinates of sampling stations can be found in the Supplementary Excel file accessible via https://doi.org/10.6084/m9.figshare.22117865.

Tableau 1. Summary of sampling campaigns and number of samples collected from each campaign.

Season	Year	Dates	Number of samples
Spring	2018	June 20–July 8	71
	2019	June 17–July 3	29
Summer	2018	August 1–18	81
	2019	July 3–August 16	218
	2021	June 28–August 20	100
Fall	2018	September 10–30	41
Winter	2018	March 1–13	62
	2019	February 23–March 14	91
	2020	February 25–March 16	73
Total			766

Sampling was carried out aboard freighter canoes guided by Cree land users during ice-free seasons and by helicopters during winters. Winter sampling was done through an auger-drilled ice hole. Sampling stations were chosen to gather data on different water masses (e.g., major river plumes) while covering the latitudinal gradient along the coast. Owing to constraints of logistic, weather, and/or ice conditions, the number and positions of the stations sampled often differed among different cruises. At all stations, profiles of water temperature and practical salinity were measured using an SBE 19plus V2 CTD (Sea Bird) or a CastAway CTD (SonTek). Water samples were collected with a 5-L Niskin bottle from the surface (~0.5 m depth) and occasionally from under the pycnocline when the water column was relatively

deep (> 5 m). A total of 766 samples were taken and 80 of them were from under the pycnocline. The number of samples from each campaign is shown in Table 1.

CDOM samples were transferred from the Niskin bottle into 120-mL borosilicate glass bottles with Teflon-lined caps and then low vacuum-filtered through Nanopure water-rinsed 0.2-µm Supor® polyethersulfone membranes (Pall Laboratory) within hours in a land-based laboratory. The filtered samples were collected into 60-mL clear borosilicate glass bottles with Teflon-lined caps and stored at 4°C in the dark until analysis within one month of sample collection. DOC samples were filtered on the field through pre-combusted (450ºC for 5 h) Whatman GF/F syringe filters (nominal pore size: 0.7 µm), transferred into 9-mL clear borosilicate vials with silicone-septum caps, acidified with HCl (2 M, 100 µl), and conserved at 4°C in the dark. During the winter expeditions, CDOM and DOC samples were quickly transferred from the Niskin bottle into sealable Whirl-Pack® bags and then brought to the land-based laboratory for filtration due to freezing temperatures on the field. Although the filter pore sizes for filtration of CDOM (0.2 µm) and DOC (0.7 µm) was different, previous studies have shown negligible differences in using 0.7-µm and smaller pore-size (0.3 or 0.2 µm) filtration for separating dissolved and particulate organic carbon (Denis *et al*., 2017; IOCCG, 2021). We used the commonly accepted GF/F filtration method for DOC analysis in order to facilitate the comparison of our DOC data with those from earlier studies. Discrete salinity samples and water stable oxygen isotope ($\delta^{18}O$-H_2O) samples were collected directly from the Niskin bottle into high-density polyethylene vials. The $\delta^{18}O$-H_2O samples were sufficiently overflowed and capped without headspace. Additional salinity samples were collected into 500-mL type III glass salinity bottles for the CTD calibration. Salinity and $\delta^{18}O$-H_2O samples were stored in the dark at room temperature until analysis. All bottles were sealed with Parafilm® to ensure the integrity of the samples. Prior to sampling, all plasticware had been acid-cleaned and all glassware had been acid-cleaned, combusted at 450°C for 5 h, and thoroughly rinsed with Nanopure water. The filters and sterile Nasco Whirl-Pak® bags had been confirmed to be free of CDOM and DOC contamination.

1.5.3 Analysis

DOC concentrations were measured using a Shimadzu TOC-V_{CPN} analyzer calibrated with potassium biphthalate. The analyzer was checked at intervals of seven consecutive sample analyses against Nanopure water (Barnstead Nanopure Infinity) and deep seawater reference produced by the Hansell's consensus reference materials (CRM) program. The highest and lowest concentrations of five injections were excluded and the average concentration was calculated on the three remaining measurements. The mean coefficient of variation on the three replicate injections was 0.5%.

CDOM absorbance spectra were scanned from 800 to 200 nm at 1-nm increments using a Perkin-Elmer Lambda-35 dual beam UV-visible spectrophotometer fitted with 1- or 5-cm quartz cells and referenced to Nanopure water. A baseline correction was applied by subtracting the average absorbance value between 683 and 687 nm from all spectral values (Babin *et al*., 2003). The 683-687 nm wavelength range was chosen because of minimal salinity and temperature effects on the absorbance over this range (Pegau *et al*., 1997; Babin *et al*., 2003). The Napierian absorption coefficient of CDOM at wavelength λ, $a_{CDOM}(\lambda)$ (m^{-1}), was calculated as 2.303 times the absorbance divided by the cell's pathlength in meters. The absorption coefficient at 440 nm, $a_{CDOM}(440)$, was chosen to represent CDOM abundance since 440 nm are the optimal wavelength for retrieving a_{CDOM} from space in Quebec's coastal waters, including the eastern James Bay (Mabit *et al*., 2022). Absorption coefficients at other commonly used wavelengths (254, 325, 330, 350, 355, 375, 412, and 443 nm) are provided in the Supplementary Excel file accessible via https://doi.org/10.6084/m9.figshare.22117865. The spectral slopes of CDOM absorption spectra between 275 nm and 295 nm ($S_{275-295}$) and between 300 nm and 650 nm ($S_{300-365}$) were calculated by nonlinear fitting $a_{CDOM}(\lambda)$ to wavelength with the exponential decay model within the respective wavelength ranges (Stedmon and Markager, 2001). The specific absorption coefficient at 254 nm, a^*_{CDOM} (254), was computed by normalizing $a_{CDOM}(254)$ by DOC concentration. We also calculated the spectral slope ratio SR (i.e., $S_{275-295}/S_{350-400}$) and the E2/E3 quotient (i.e., $a_{CDOM}(250)/a_{CDOM}(365)$), both of which are indicators of the molecular

weight of CDOM (De Haan and De Boer, 1987; Helms *et al*., 2008). Since $S_{275\text{-}295}$ is also an indicator of the CDOM molecular weight (Helms *et al*., 2008) and is significantly correlated to SR (Pearson's R = 0.896) and E2/E3 (Pearson's R = 0.959) (Supplementary Table S1), we chose to only present $S_{275\text{-}295}$ in the main text to minimize redundancy. Readers interested in the SR and E2/E3 data are referred to the Supplementary Excel file.

Discrete salinity samples were measured on the field using a Cond 330i conductivity meter (WTW) calibrated against a KCl solution (1413 µs/cm). Salinity samples for the calibration of the CTD were analyzed using an 8410A Portasal salinometer (Guildline Instruments). The conductivity meter-determined salinities agreed well with the salinometer-determined salinities (conductivity meter = 0.99 × salinometer + 0.04, R^2 = 0.95) and with the CTD-determined salinities (conductivity meter = 1.00 × CTD – 0.26, R^2 = 0.95).

The $\delta^{18}O\text{-}H_2O$ samples were analyzed using a Micromass model Isoprime DI isotope ratio mass spectrometer (Elementar, Ronkonkoma, NY, USA) coupled to an AquaPrep system (Langenselbold, Germany) (precision = ± 0.1‰) in the UQAM-GEOTOP laboratory. Raw values were corrected using three reference standards on a VSMOW-SLAP scale. Instrument performance and stability were evaluated with a fourth reference water (Barbecot *et al*., 2018).

Mixed models were performed in R version 4.2.2 using lme4 and lmertest packages (Bates *et al*., 2014; Kuznetsova *et al*., 2015) to investigate relationships between salinity, a_{CDOM}, spectral slopes and $\delta^{18}O\text{-}H_2O$ across regions and seasons, with traplines and years as random effects. These models allow for control on differences in sampling locations and interannual variability. Considering the distinct separation of stations north and south of the LGR in the $a_{CDOM}(440)$-vs.-salinity plots (Section 1.6.3), a mixed model was performed to see if the southern stations were statistically different from the northern stations (including stations in and off the LGR). Seasonal differences were then investigated among these regions. Stations with salinity < 0.2 were excluded from the salinity-vs.-$a_{CDOM}(440)$ models to isolate river endmembers and consequently significantly increase the R^2 and better fit the model assumptions. Southern stations proximal to the LGR were also excluded from the

analysis as they do not fall consistently in the northern or southern regression lines (i.e., depending on the season). All data points excluded from the regressions are still reported on the plots. Supplementary Table S2 summarizes the fitted parameters of all mixed models performed and marginal R^2 are reported in their respective figures. A post-hoc Tukey test was performed when the relationships across seasons were statistically different (Supplementary Table S3).

1.6 RESULTS AND DISCUSSION

1.6.1 General hydrographic setting

Surface-water temperature exhibited strong seasonality, increasing from the winters (range: −1.3–0.5 °C; mean: −0.3 °C) to the springs (range: 0.8–19.7 °C; mean: 6.9 °C) to the summers (range: 2.2–21.1 °C; mean: 11.5 °C) and then decreasing to the fall (range: 5.3–10.0 °C; mean: 7.8 °C) (Supplementary Figure S1). During all seasons, surface-water salinity was lowest around the mouth of the LGR, with its plume most extensive during the winters and most restrictive during the springs and summers (Supplementary Figure S1), in line with the LGR's seasonal freshwater discharge trend (de Melo *et al*., 2022). In contrast, the flows in the unregulated rivers (URRs) troughed in the winters due to snow accumulation and peaked in the springs due to snow melting (de Melo *et al*., 2022). The water was mostly stratified when the water column was sufficiently deep (> 5 m) (data not shown).

The $\delta^{18}O$-H_2O–salinity relationship generally showed little deviation from the conservative mixing line (Figure 6), suggesting that freshwater input was dominated by discharge from several major rivers in the region, with a negligible contribution from ice melting. This pattern was found year-round as evidenced by the lack of statistical differences in the relationship across seasons (Supplementary Table S2). The intercept of −13.93‰ combining all seasons is in the range of other river endmembers in Hudson Bay (−19.5–−10.3‰, Granskog *et al*., 2011) and the extrapolation of the relationship yields a seawater endmember of −1.79‰, which is very similar to what was found in Hudson Bay for an

equivalent salinity measurement (−1.5 ± 0.2‰ at salinity of 32.8; Granskog *et al*., 2011). The deviation of several points from the mixing line at relatively high salinities (> 20) might reflect the influence of brine rejection during ice formation (points below the line) or sea ice melting (points above the line) at a few stations away from the shore. The relationships between $\delta^{18}O$-H_2O and salinity found in our study contrast the patterns found in Hudson Bay, which have shown significant scattering along the mixing line reflecting the influence of sea ice (Granskog *et al*., 2009). Indeed, some studies have shown that ice melting can significantly contribute to the freshwater budget during spring and early summer in James Bay and Hudson Bay (Prinsenberg, 1988; Landy *et al*., 2017). However, this surface freshening by sea-ice melt is restricted to the offshore areas whereas the coastal freshening is largely controlled by riverine runoff in Hudson Bay (Granskog *et al*., 2011). On the other hand, the freshwater discharged from rivers has been shown to follow the coastline with little mixing with offshore waters in both Hudson Bay and James Bay (Granskog *et al*., 2011; Meilleur *et al*., 2023), therefore contributing to the important riverine signature at the coastal stations. Moreover, our spring sampling (mid-June to early July) was conducted after the major sea ice melting period (mid-May to mid-June) (Table 1), further diminishing the contribution of sea ice melting to the freshwater budget in the sampling area. As water sampling was carried out on board Cree's small freighter canoes, safety concern was a critical factor in deciding the timing of the spring field campaigns to avoid complex ice conditions.

The hydroelectric development in the region increased the importance of the eastern James Bay river inputs to the freshwater budget of the bay, which may contribute to the highly terrestrial nature of the region. The extensive watershed manipulations not only changed the timing and the amount of freshwater input into the James Bay itself, but also diverted freshwater from the nearby Ungava Bay watershed (Figure 4). More precisely, the Caniapiscau River was diverted of 748 $m^3\ s^{-1}$ of its flow (about 45% flow reduction at the mouth) (Déry *et al*., 2016) totaling 9% of the whole eastern James Bay freshwater export nowadays (227 $km^3\ year^{-1}$), consequently contributing to the marked influence of terrestrial inputs on the James Bay marine ecosystem. Our results highlight the need to contrast the contribution of sea ice to the freshwater budget in James Bay from Hudson Bay.

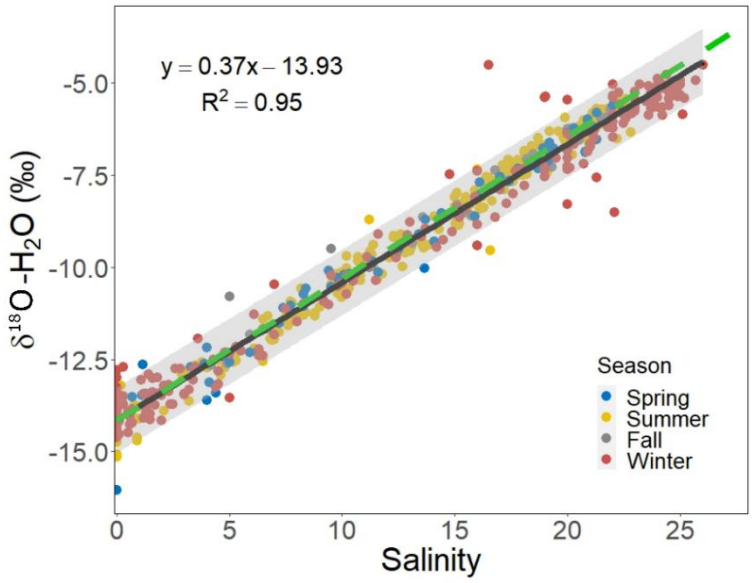

Figure 6. Relationship between surface $\delta^{18}O$-H_2O and salinity for different seasons. The solid black line represents the linear fit to the composite data. The shaded area denotes the 95% prediction band of the linear fit. The dashed green line represents the mixing line connecting our average river endmember and the seawater endmember reported by Granskog *et al.* (2011).

1.6.2 River endmembers

Figure 7 compares the mean absorption spectra of CDOM collected from the regulated LGR, the URRs, and marine waters. The mean a_{CDOM} of the URRs was higher than that of the LGR over the UV and visible wavelengths from 250 to 600 nm; in turn, the mean a_{CDOM} of the LGR exceeded that of the marine waters with salinities > 23. However, both the absolute and relative differences between the URRs and the LGR were greater than those between the LGR and the marine waters. In addition, the relative difference, as expressed by the absorption ratio, generally increased with wavelength, from 2.61 at 250 nm to 3.19 at 600 nm between the URRs and the LGR and parallelly from 1.54 to 2.00 between the LGR and the marine waters. This result suggests that the concentrations of the visible light-absorbing chromophores in CDOM are lowest in marine waters, intermediate in the LGR, and highest in the URRs.

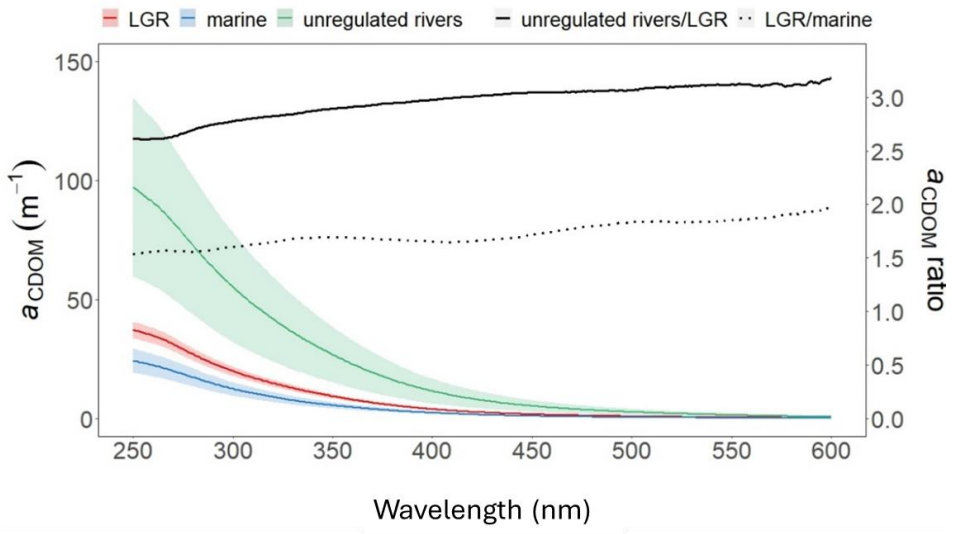

Figure 7. Mean CDOM absorption spectra for the La Grande River (LGR) stations with salinity < 0.2 (red) (n = 46), unregulated rivers (URRs) stations with salinity < 0.2 (green) (n = 24) and marine water stations with salinity > 23 (blue) (n = 50), and absorption coefficient ratios of URRs to LGR (solid black line) and LGR to marine water (dotted black line). The shaded area denotes one standard deviation.

The river endmembers of DOC and $a_{CDOM}(440)$ spanned from 3.80 to 13.68 mg L^{-1} and 1.80 to11.69 m^{-1}, respectively, across all sampled rivers, with the mean values for the URRs being 2.50 (DOC) and 3.35 ($a_{CDOM}(440)$) times those for the LGR (Table 2). The mean $S_{275-295}$ and $a^*_{CDOM}(254)$ for the URRs were 10.6% lower and 11.7% higher than those for the LGR, respectively, suggesting that DOM in the URRs were slightly enriched with high-molecular-weight and aromatic moieties relative to DOM in the LGR, consistent with the enhancement of the visible-light a_{CDOM} in the URRs vs. in the LGR noted earlier. The much lower DOC and $a_{CDOM}(440)$ for the LGR could be attributed to its longer water residence time due mainly to ten reservoirs (total volume 170 km^3) that were built in the LGR watershed, which increases microbial and photochemical removal of DOM (Battin *et al*., 2008). While photochemical processing tends to increase $S_{275-295}$ and diminish $a^*_{CDOM}(254)$ of the remaining DOM pool, microbial processing often leads to an opposing outcome (Helms *et al*., 2008; Hansen *et al*., 2016). This may partly explain the large differences in DOC and $a_{CDOM}(440)$ but much smaller dissimilarities in $S_{275-295}$ and $a^*_{CDOM}(254)$ between the LGR and the URRs (Table 2).

Tableau 2. River endmembers (salinity < 0.2) of DOC, $a_{CDOM}(440)$, $S_{275\text{-}295}$, and $a^*_{CDOM}(254)$. NA: not available; SD: standard deviation; RSD: relative standard deviation (i.e., (SD/mean)*100); Sp: spring; Su: summer; W: winter.

River	Season/year	DOC (mg L^{-1})	$a_{CDOM}(440)$ (m^{-1})	$S_{275\text{-}295}$ (μm^{-1})	$a^*_{CDOM}(254)$ (L mg^{-1} m^{-1})	$\delta^{18}O\text{-}H_2O$ (‰)
Regulated river						
La Grande	Sp/2018	4.45	2.05	15.25	7.73	−13.96
	Sp/2019	NA	1.8	15.58	NA	−14.17
	Su/2018	3.82	1.98	15.39	9.68	−13.94
	Su/2019	3.8	1.88	15.69	9.19	−14.22
	Su/2021	3.89	2.18	14.8	9.95	−14.6
	W/2018	3.9	2.16	15.13	10.01	−13.9
	W/2019	3.82	1.93	15.57	9.6	−14.16
	W/2020	NA	1.92	15.32	NA	−14.47
Range		3.80 – 4.45	1.80 – 2.18	14.80 – 15.69	7.73 – 10.01	−14.60 – −13.90
Mean		3.95	1.99	15.34	9.36	−14.18
SD		0.25	0.13	0.29	0.85	0.25
RSD (%)		6.3	6.7	1.9	9.1	1.8
Unregulated rivers						
Roggan	W/2018	6	3.12	15.57	9.8	−12.99
	W/2019	11.51	5.16	15.32	7.63	−13.84
Piagochioui	W/2018	8.54	5.34	13.56	9.75	−13.4
Caillet	Su/2021	13.33	10.59	11.84	10.99	−13.22
Castor	Sp/2018	9.18	5.85	14.17	10.55	−13.98
	W/2018	9.59	6.63	13.93	11.13	−13.43
	W/2019	9.54	6.06	14.98	10.45	−13.42
	W/2020	8.92	NA	NA	NA	−13.91
Maquatua	Sp/2018	8.91	5.92	14.35	10.86	−13.79
	Su/2019	8.88	5.37	13.79	10.49	−14.47
	W/2018	10.85	6.99	14.27	10.41	−12.81
	W/2020	9.3	5.11	14.56	9.55	−13.41
Old Factory	Sp/2018	8.45	5.82	14.03	10.6	−13.55
	W/2020	8.41	5.97	13.39	10.71	−13.7
Eastmain	Su/2019	10.73	8.43	13.16	11.98	−15.08
	W/2018	13.68	11.69	11.7	11.59	−13.25
	W/2020	12.04	8.62	12.66	10.82	−13.57
Range		6.00 – 13.68	3.12 – 11.69	11.70 – 15.57	7.63 – 11.98	−15.08 – −12.81
Mean		9.87	6.67	13.83	10.46	−13.64
SD		1.94	2.18	1.11	0.98	0.54
RSD (%)		19.7	32.7	8	9.4	4

DOC and the three optical metrics in the LGR had rather small relative standard deviations (RSD) (range: 1.9–9.1%, Table 2). Furthermore, two-tail t-tests showed no significant seasonal variations for all four variables ($0.559 \leq p \leq 0.720$) and no significant interannual variations (2018 vs. 2019) for DOC ($p = 0.339$) and $a^*_{CDOM}(254)$ ($p = 0.763$) at α of 0.05. The $a_{CDOM}(440)$ ($p = 0.040$) and $S_{275\text{-}295}$ ($p = 0.024$) displayed borderline significance in interannual variation at α of 0.05 but insignificance at α of 0.01. Overall, these results signify relatively stable concentrations and quality of the LGR DOM endmember. This temporal stability could be due partly to the water residence time in the LGR reservoirs being more than one year (i.e., the reservoir water volume of 170×109 m^3 divided by the annual water discharge rate of 3446 m^{-3} s^{-1} = 1.56 years), which dampens potential seasonal variations.

The URRs varied from 6.00 to 13.68 mg L^{-1} in DOC and from 3.12 to 11.69 m^{-1} in $a_{CDOM}(440)$, with the lower bounds observed in the Roggan River and the upper bounds in the Eastmain River (Table 2). In addition to the across-river variations, some rivers also exhibited substantial seasonal (Maquatua: spring 2018 vs. winter 2018) and interannual (Roggan: winter 2018 vs. winter 2019; Maquatua and Eastmain: winter 2018 vs. winter 2020) changes in DOC and $a_{CDOM}(440)$. On a multiple-years and across-rivers basis, the summer showed the highest mean $a_{CDOM}(440)$ (8.13 m^{-1}) followed by winter (6.47 m^{-1}) and spring (5.86 m^{-1}) but one-way Analysis of Variance (ANOVA) tests indicated that the differences among the three seasons were insignificant ($p = 0.426$) at the significance level (α) of 0.05. $S_{275\text{-}295}$ and $a^*_{CDOM}(254)$ for the URRs ranged from 11.70 to 15.57 μm^{-1} and 7.63 to 11.98 L mg^{-1} m^{-1}, respectively, with the Roggan River displaying relatively higher $S_{275\text{-}295}$ and lower $a^*_{CDOM}(254)$ while the Eastmain River manifesting the opposite (Table 2). Overall, the variabilities of $S_{275\text{-}295}$ (RSD: 8.0%) and $a^*_{CDOM}(254)$ (RSD: 9.4%) were far smaller than those of DOC (RSD: 19.7%) and $a_{CDOM}(440)$ (RSD: 32.7%), demonstrating smaller changes in the nature of DOM across the UURs compared to the variations in DOM abundance.

The LGR and URRs endmembers, taken together, revealed a linear decrease in $S_{275\text{-}295}$ and increase in $a^*_{CDOM}(254)$ with rising $a_{CDOM}(440)$ (Supplementary Figure S2), despite their

far smaller spatiotemporal variabilities relative to those in $a_{CDOM}(440)$ and DOC. This observation implies that the molecular weight and aromaticity of DOM across these rivers increase with its color, which could be partly linked to the different watershed landscape compositions of the rivers (Fink-Mercier *et al*., 2022).

1.6.3 Spatiotemporal distributions of CDOM

The distributions of CDOM were delineated using $a_{CDOM}(440)$-vs.-salinity plots instead of conventional spatial distribution maps, given 1) the patchy distribution of sampling stations, often clustered around the river mouths (Figure 5), 2) the inconsistency of the station distributions among the different cruises (Figure 5), and 3) the strong but spatially variable impact of terrestrial input on CDOM in the study area.

The entire dataset for all cruises combined manifests linear decreases in $a_{CDOM}(440)$ with increasing salinity, indicating a seaward decline of CDOM throughout the sampling area and seasons (Figure 8). Notably, two distributional patterns increasingly diverged towards low salinities but converged towards high salinities. These two statistically different patterns (Supplementary Table S2) separated the sampling stations into two groups: one located off and north of the LGR (> 54 ºN) and the other south of the LGR (< 53.5 ºN) (Figures 4 and 8), demonstrating the regional influence of this river on the whole northern sector of the coast. We define hereafter these two groups as the LGR-influenced area and the URRs-influenced area. The fitted slope for the URRs-influenced area (–0.28 ± 0.01) was six times that for the LGR-influenced area (–0.05 ± 0.01; Supplementary Table S2) because of the much higher CDOM endmembers of the URRs (Table 2). However, the CDOM signature of the LGR, due to its large freshwater discharge (Figure 8), was conspicuous as far as the northernmost sampling stations near Hudson Bay despite other smaller rivers releasing CDOM-richer freshwater into the northern James Bay (e.g., the Roggan and the Piagochioui, Figure 8 and Table 2). In fact, the LGR's terrestrial signal has previously been detected in as far as the northern Hudson Bay (Meilleur *et al*., 2023).

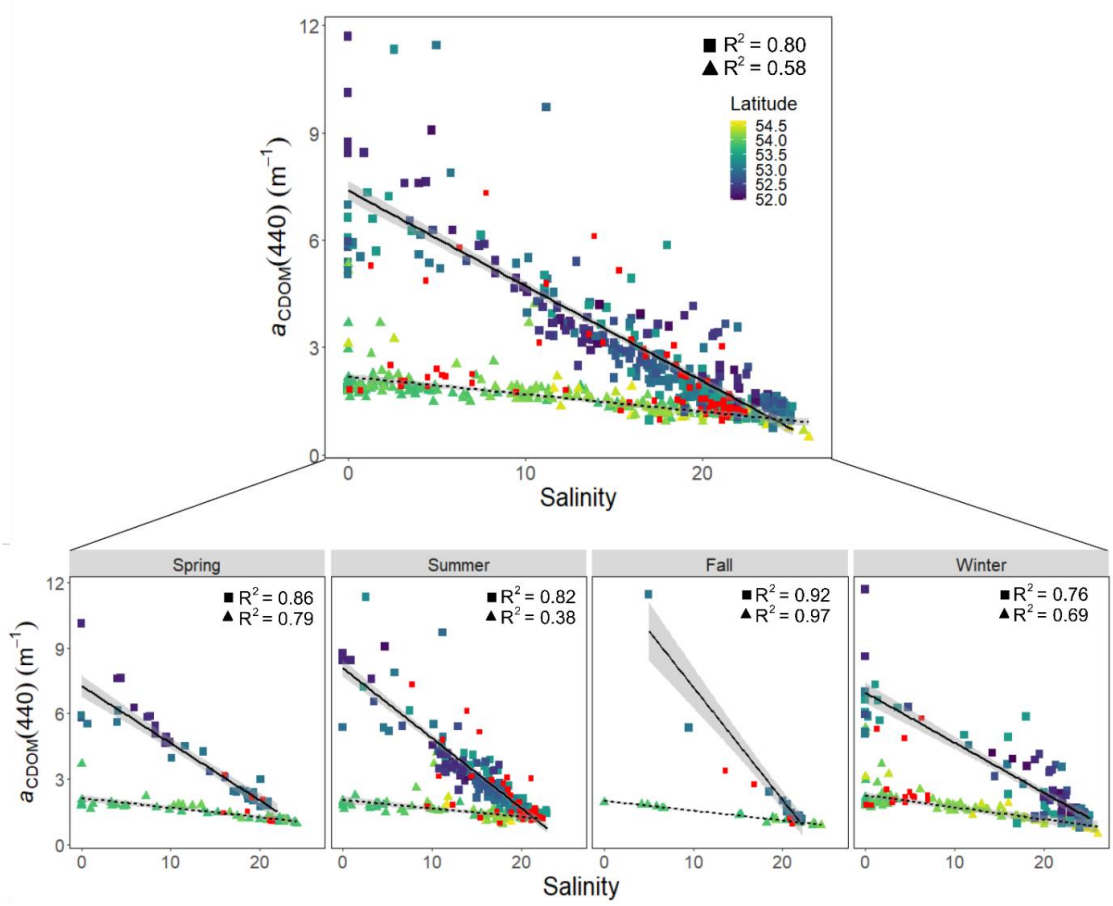

Figure 8. Relationship between $a_{CDOM}(440)$ and salinity for all cruises combined (top) and for each season (bottom). The dashed lines represent the regression lines for the stations of the LGR plume and north of the LGR (triangles) and solid lines represent the regression line for the stations south of the LGR (non-red squares). The shaded areas represent the 95% confidence interval. The color scale represents the latitude (°N). Red squares represent stations directly south of the LGR excluded from the regressions (see Methods). River endmembers were excluded from the regressions but reported on the plots.

Considering that the data is divided into the LGR-influenced area and the URRs-influenced area, individual seasonal relationships for the two regions were investigated. Only the URRs-influenced area exhibited some seasonally different relationships (Figure 8, Tables S1 and S2), with notably the summer bearing a steeper slope (−0.33 ± 0.02) compared to winter (−0.22 ± 0.02) ($p < 0.0001$). This pattern likely reflected differences in riverine inputs as shown by the accompanying higher CDOM endmembers in summer as noted earlier (Table 2). Indeed, periods of higher flow related to higher surface runoff has been shown to

correspond to greater terrestrial DOM contribution in major Arctic rivers (Spencer *et al*., 2009; Griffin *et al*., 2018; Johnston *et al*., 2021). The absence of seasonal relationships in the LGR-influenced area reflect the regulated flow and the long residence time in the reservoirs leading to relatively flattened hydrograph and consequently lower seasonality in freshwater and CDOM inputs year-round compared to other rivers in the region (Déry *et al*., 2016). The regulated Nelson River that flows into western Hudson Bay also exhibits little seasonality in water isotopes and CDOM, which has been similarly attributed to its relatively steady flow (Smith *et al*., 2015; Meilleur *et al*., 2023).

Outliers identified in Figure 8 are mainly stations in the vicinity of the LGR plume between the La Grande and Caillet rivers (Figure 4). These stations belong in theory to the southern group. Yet since they were sometimes covered by the LGR plume depending on the season, they could not be assigned to either the URRs- or LGR-influenced area. The LGR plume varies widely across seasons (Peck *et al*., 2022), being restricted to the river mouth during the summer, but reaching as far as the Caillet River in the winter (Figure S1). These so-called outliers, nevertheless, fall into one of the two distribution patterns, regardless of the season, indicating that they are influenced by either the URRs- or LGR-influenced water masses.

The absorption coefficient of CDOM in our study ranged from 2.22 to 50.02 m^{-1} (mean: 10.29 m^{-1}) at 350 nm, 2.03−48.85 m^{-1} (mean: 9.87 m^{-1}) at 355 nm, 0.48–11.69 $m^{-}1$ (mean: 2.31 m^{-1}) at 440 nm and 0.45–11.19 m^{-1} (mean: 2.30 m^{-1}) at 443 nm (Supplementary Excel file accessible via https://doi.org/10.6084/m9.figshare.22117865). The ranges compare well with $a_{CDOM}(350)$ found in other estuarine and coastal systems around the globe (0.5–55 m^{-1}) (Massicotte *et al*., 2017) and with $a_{CDOM}(355)$ in the Hudson Bay system (0.11–32.33 m^{-1}) (Guéguen *et al*., 2011, 2016; Meilleur *et al*., 2023), although the latter has somewhat lower values. Our absorption coefficients at 440 nm are, however, much higher than those in the central-eastern Arctic surface waters including part of the outer shelf of the Laptev Sea (range: 0.09–1.04 m^{-1}, mean: 0.32 m^{-1} at 443 nm; Goncalves-Araujo *et al*., 2018)

likely due in part to the more river-impacted nature of the eastern James Bay and in part to the more coastal nature of the sampling area in the present study.

1.6.4 Mixing behavior of CDOM

The linear relationships of $a_{CDOM}(440)$ to salinity (Figure 8), alongside the strong, positive correlations of a_{CDOM} at the UV wavelengths with $a_{CDOM}(440)$ (Supplementary Table S1), indicates that the distribution of CDOM in the eastern James Bay was primarily controlled by physical mixing of high-CDOM river water with low-CDOM offshore bay water. Note that the under-pycnocline $a_{CDOM}(440)$ data points well follow the CDOM-salinity trends established by the surface data (Supplementary Figure S3), suggesting that the deeper CDOM was largely controlled by downward transport from surface water instead of upward input from underlying sediments. This dominance of physical mixing in the control of CDOM distribution indicated that other processes, such as flocculation and photochemical and microbial degradation, only played minor roles. CDOM photodegradation in seasonally ice-covered waters is favored in summer due to ice-free conditions permitting deeper penetration of solar radiation into the water column and to warmer temperatures increasing the efficiency of the photodegradation process (Zhang *et al*., 2006; Song *et al*., 2017). The warmer temperatures in summer should also promote microbial degradation. The lack of significant CDOM removal year-round, including during the ice-free, warmer summer seasons, could result from the short residence times of the LGR-dominated river water in the eastern James Bay (several days in summer and several weeks in winter) (Guzzi, 2022), which might have prevented significant photochemical and microbial processing of CDOM from taking place before CDOM was transported out of the bay. Previous studies have shown that DOM remained largely unchanged during its transit from James Bay to the southern Hudson Bay, reflecting its rapid transport and limited degradation (Granskog *et al*., 2009; Meilleur *et al*., 2023).

In seasonally sea ice-covered water bodies, the formation and melting of sea ice may also affect CDOM dynamics. Sea ice formation rejects CDOM along with salts into the water

column, while sea ice melting may dilute CDOM in the underlying seawater (Jørgensen *et al*., 2015) or release fresh, ice algae-derived DOM, including CDOM, into the water column (Norman *et al*., 2011; Xie *et al*., 2014; Brogi *et al*., 2018), thereby potentially generating different endmembers in the respective seasons. In James Bay, sea ice usually starts to form in December and melt in May (Taha *et al*., 2019). Figure 8 indicates conservative mixing behaviors of CDOM in different seasons in the nearshore eastern James Bay, except a few winter data points for the URRs-influenced area showing upward deviations at salinity ~20 that might result from CDOM release into seawater linked to brine rejection during ice formation (Section 1.6.1). The CDOM conservative behaviors imply minor effects of sea ice formation and melting on the CDOM dynamics, which is supported by the $\delta^{18}O$-H_2O data manifesting an overall absence of significant amounts of brine or sea ice meltwater in the sampled areas. As elaborated in Section 1.6.1, the paucity of brine or sea ice meltwater could be attributed to the water circulation patterns in James Bay and the mismatch between the sea ice melting and water sampling periods. This information further reinforces the earlier argument (Section 1.6.3) that the steeper slope of the $a_{CDOM}(440)$-vs.-salinity relationship for the URRs in summer compared to winter was due to higher riverine CDOM inputs instead of dilution of CDOM by ice meltwater during summer.

The fitted intercepts of the linear regression lines (Supplementary Table S2) represent the composite river endmembers of $a_{CDOM}(440)$. The all cruises-inclusive composite endmembers derived in this manner are 2.18 m^{-1} for the LGR and 7.64 m^{-1} for the URRs (Table S2), close to the mean measured river endmembers of 1.99 m^{-1} and 6.67 m^{-1}, respectively (Table 2), despite the exclusion of the river endmembers (salinity < 0.2) from the regression analysis (Section 1.5.3). Although the composite river endmember of $a_{CDOM}(440)$ shows little seasonality for the LGR, it does exhibit significant differences among certain seasons for the URRs (Supplementary Tables S1 and S2), which again conforms to the more variable measured river endmembers for the latter (Table 2). Regardless of this seasonal variability for the URRs, the $a_{CDOM}(440)$–salinity relationships for the LGR- and URRs-influenced areas always converge around salinity 25 (Figure 8). Similar relationships converging to a unique marine endmember have been found in Hudson

Bay estuaries (Guéguen *et al*., 2011; 2016) and other estuarine systems with low salinity (Coble, 2007; Granskog *et al*., 2007; Asmala *et al*., 2016), spurring the use of CDOM absorption coefficients as tracers of freshwater in these systems (Granskog *et al*., 2007).

The mixing of river water with seawater impacted CDOM not only quantitatively (Figure 8) but also qualitatively. $S_{275\text{-}295}$ augmented and $a^*_{CDOM}(254)$ declined with decreasing $a_{CDOM}(440)$ (i.e., increasing salinity) (Figure 9 a,b), indicating that the molecular weight and aromaticity of CDOM diminished during the seaward transport. Because CDOM absorption behaved conservatively, the seaward changes in $S_{275\text{-}295}$ and $a^*_{CDOM}(254)$ should primarily result from the dilution of riverine CDOM by seawater containing CDOM relatively depleted with high-molecular-weight and aromatic moieties. This differs from the observation in Hudson Bay where a loss of CDOM absorption and changes in spectral slopes in surface waters have been spotted and attributed in part to CDOM photobleaching (Granskog, 2012). Although marginal differences in the $S_{275\text{-}295}$–$a_{CDOM}(440)$ and $a^*_{CDOM}(254)$–$a_{CDOM}(440)$ relationships exist among certain seasons and between the LGR- and URRs-influenced areas ($a^*_{CDOM}(254)$ only) (Supplementary Figure S4, Tables S2 and S3), the overall trend of either metrics revealed by its composite data combining all cruises and both regions can be well described by a single mathematical form (Figure 9a,b). Notably, no distinct regional patterns were identified, in contrast to the $a_{CDOM}(440)$–salinity relationship (Figure 8) but consistent with the finding that the differences in the river endmembers of $S_{275\text{-}295}$ and $a^*_{CDOM}(254)$ between the LGR and URRs are far smaller than that in the river endmember of $a_{CDOM}(440)$ (Table 2). The $a_{CDOM}(440)$ can thus be used as an indicator of the quality (molecular weight and aromaticity) of CDOM in the eastern James Bay with little seasonal and regional restrictions.

The lack of removal of riverine CDOM during physical mixing suggested that the CDOM pool in the eastern James Bay could be primarily of terrestrial CDOM origin. This speculation was assessed using the $S_{300\text{-}650}$–$a_{CDOM}(375)$ relationship that has been frequently used for differentiating marine and terrestrial CDOM (Stedmon and Markager, 2001). The composite data from the present study shows little variation in $S_{300\text{-}650}$ with increasing

$a_{CDOM}(375)$ except for the initial mild decline (Figure 10). All the $S_{300-650}$ values are far above the marine CDOM region modeled by Stedmon and Markager (2001), demonstrating the dominance of the terrestrial signature in the eastern James Bay.

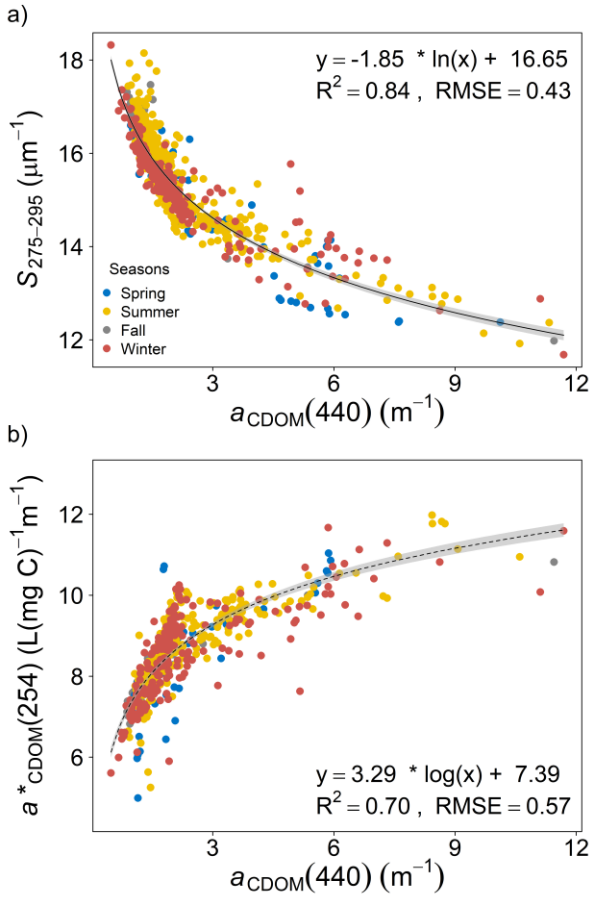

Figure 9. Relationships between $S_{275-295}$ and $a_{CDOM}(440)$ (a) and $a^*_{CDOM}(254)$ and $a_{CDOM}(440)$ (b) for different seasons. Solid black line represents the fit of the composite data to the simple logarithmic function. The shaded area denotes the 95% confidence interval of the regression fit. See Table S2 for the values of the fitted parameters and Table S3 for the results of the post-hoc Tukey test. RMSE: root mean square error. Similar plots with color bar showing latitude are presented in Supplementary Figure S4.

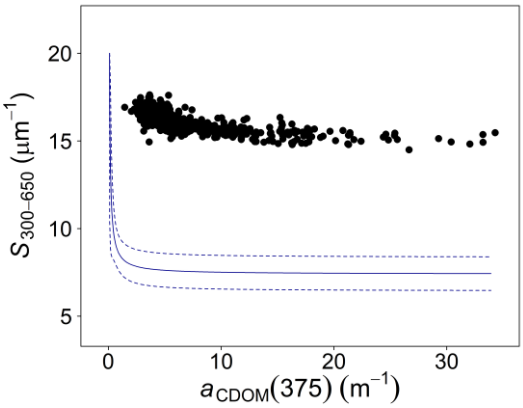

Figure 10. Scatter plot of $S_{300-650}$ against $a_{CDOM}(375)$ for the composite data from all cruises. The solid blue line represents the SM01 (Stedmon and Markager, 2001) model for marine CDOM that is delimited by the dashed blue lines.

1.6.5 CDOM as an indicator of DOC

DOC concentration showed a strong linear correlation to $a_{CDOM}(440)$ (Figure 11a), with the concentrations calculated from the fitted equation generally agreeing with the measured ones within the 95% prediction band (Figure 11b; mean RSD: 5.3%). This robust correlation, alongside the similarity of the DOC– and $a_{CDOM}(440)$–salinity relationships (Figures 8 and Supplementary Figure S5), suggested that the two variables covaried in the eastern James Bay. Indeed, DOC and CDOM are frequently coupled in estuaries and rivers (Coble, 2007; Spencer *et al.*, 2007; Massicotte *et al.*, 2017; Griffin *et al.*, 2018), pointing to common loading and removal processes in these ecosystems. The relationship between DOC and $a_{CDOM}(440)$ exhibited little seasonal and interannual variabilities as previously shown in other estuaries with peatland-derived river inputs (Tyne and Tweed estuaries) (Spencer *et al.*, 2007). In fact, only the winter relationship was marginally different from the spring (Supplementary Table S3). Yet, since these two seasons had widely different spatial coverages (Figure 5), it is difficult to suggest an underlying mechanism related to differential loading or loss. In contrast, other studies have shown clear seasonal trends that the authors attributed to seasonal hydrological changes influencing DOM sources associated to flow paths (Harvey *et al.*, 2015; Juhls *et al.*, 2020) and the processing of different organic matter

fractions (Del Vecchio and Blough, 2004; Osburn *et al*., 2016). Our results therefore support again that the eastern James Bay DOM inputs are driven by a dominant single source year-round (i.e., riverine) and that there is little degradation along the estuarine flow path. This stable DOC–CDOM relationship provides a simplified approach for estimating broader DOC budgets in the eastern James Bay from CDOM absorption coefficients, which can be relatively easily measured in strongly river-impacted coastal areas such as James Bay.

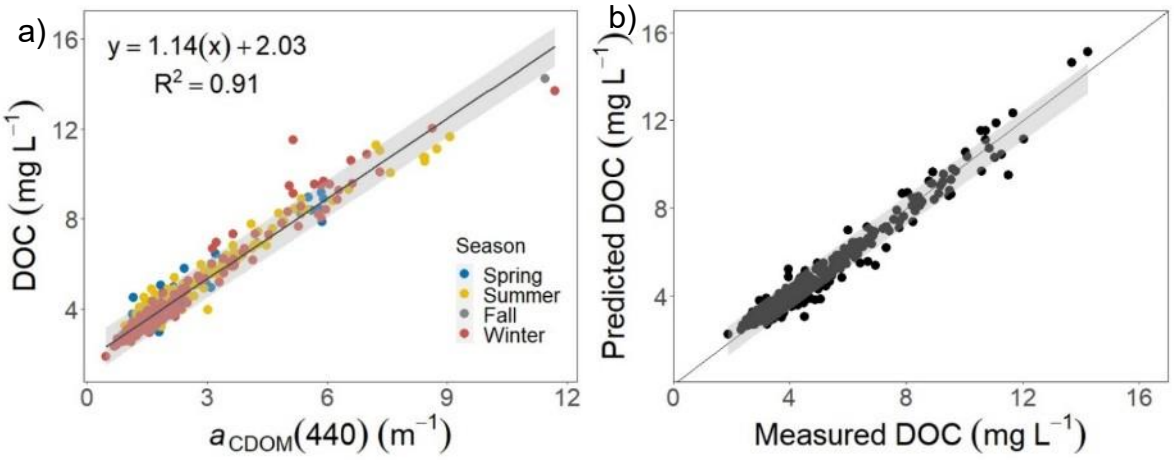

Figure 11. Relationships between $a_{CDOM}(440)$ and DOC across all seasons (a) and between DOC predicted from the DOC-vs.-$a_{CDOM}(440)$ model and measured DOC (b). The solid line represents the linear fit of the composite data in panel a and a 1:1 line in panel b. The shaded area in panel a denotes the 95% confidence interval of the linear fit and the 95% prediction band in panel b.

Furthermore, CDOM absorption coefficients and other CDOM optical properties can effectively be retrieved at large scales in optically active waters with satellite-based remote sensing (Bélanger *et al*., 2008; Aurin *et al*., 2013; Griffin *et al*., 2018). This approach has more recently been implemented in Quebec's coastal waters, including the eastern James Bay at the optimal wavelength of 440 nm (Mabit *et al*., 2022), offering the potential for estimating DOC concentrations in real time and synoptically. The validation of the remote-sensing algorithm, however, contained only a few CDOM data points with limited spatiotemporal coverage in the eastern James Bay. Here, we provide evidence that the DOC–$a_{CDOM}(440)$ relationship is robust and consistent across the whole eastern James Bay (from Rupert Bay

to Cape Jones) and is independent of seasonality. Moreover, since $a_{CDOM}(440)$ can also serve as a year-round indicator of $S_{275\text{-}295}$ and $a^*_{CDOM}(254)$ (Section 1.6.4), remote sensing may be potentially employed to monitor the quality of CDOM as well. Our results can therefore contribute to future large-scale assessment of DOM dynamics and chemical characteristics in James Bay through remote sensing.

1.7 CONCLUSIONS

Freshwater discharged from the regulated LGR is highly depleted in CDOM compared with that from the unregulated rivers on the eastern James Bay coast. Qualitatively, the two CDOM pools are only moderately different in terms of molecular weight and aromaticity as indicated by $S_{275\text{-}295}$ and $a^*_{CDOM}(254)$, respectively. We hypothesize that this quantity-quality divergence stems from longer water residence times in the ten reservoirs of the LGR watershed, allowing CDOM to undergo more extensive photochemical and microbial degradations both of which consume CDOM but each of which exerts an opposing effect on the molecular weight and aromaticity of the residual CDOM. The functionality of $S_{275\text{-}295}$ and $a^*_{CDOM}(254)$ for inferring the nature and extent of CDOM processing is thus limited in environments where photochemical and microbial degradations are similarly important in modifying the quality of CDOM.

The combination of the low CDOM endmember of the LGR with its high freshwater discharge leads to a large swath of the northern James Bay, and potentially part of the southern Hudson Bay as well, being far more light-transparent than if the LGR had not been regulated. The regulation of the LGR thus not only greatly changes the hydrodynamics and salinity distribution, but may also profoundly impact the optics, biogeochemical cycles, and ecology in James Bay. The large difference in the CDOM river endmember between the LGR and the URRs gives rise to distinct mixing patterns of the two CDOM pools that can potentially be employed for distinguishing and tracing the freshwater masses from the two river systems in the eastern James Bay. The highly conservative mixing behavior of CDOM with insignificant (the LGR-influenced area) or only marginal seasonality (the URRs-

influenced area) sets the eastern James Bay apart from many other river-impacted northern systems, which are characterized by pronounced seasonal variability of CDOM mixing dynamics.

The simple but robust linear correlation between DOC and $a_{CDOM}(440)$, with little spatiotemporal variability, will greatly simplify remote sensing of DOC in the eastern James Bay. The quantitative relationships identified between $S_{275-295}$, $a^*_{CDOM}(254)$ and $a_{CDOM}(440)$, again largely independent of seasons and regions, also allows the quality of CDOM to be potentially assessed from space. These results demonstrate the feasibility for implementing real-time and synoptical monitoring of DOM dynamics and characteristics in the eastern James Bay and possibly in the entire James Bay.

This study improves our understanding of how river regulation may affect the abundance and quality of riverine CDOM delivered to northern land-sea transitional zones and its ensuing mixing processes and biogeochemical cycles. It reveals the surprisingly low seasonal and interannual sensitivity of CDOM mixing dynamics in the eastern James Bay and highlights the implications of this temporal stability for real-time and bay-wide satellite-based assessment of DOM dynamics and more broadly the DOM-related biogeochemical cycles and ecology.

1.7.1 Data availability statement

The original data presented in the study are included in the article, the Supplementary Materials and the Excel data file at figshare.com (accessible via https://doi.org/10.6084/m9.figshare.22117865). Further inquiries can be directed to the corresponding authors.

1.7.2 Declaration of competing interest

The authors declare that they have no known competing financial interests or personal relationships that could have appeared to influence the work reported in this paper.

1.7.3 Author contributions

HX, MG, and AÉ conceptualized this research with inputs from all the other authors. All authors contributed to the design of the field sampling strategy. VG, CFM, and UN coordinated the sampling campaigns. AÉ, VG, and CFM were the main contributors to data collection. CFM and AÉ conducted data analysis and visualization. AÉ wrote the original draft based on the data of 2018 and winter and summer 2019. CFM and HX rewrote the manuscript that incorporated the data of fall 2018, spring 2019, 2020, and 2021. All the other authors commented on the manuscript.

1.7.4 Acknowledgements

We thank the Cree local coordinators Ernie Rabbitskin, Geraldine Mark and Ernest Moses, employees of Niskamoon Corporation, and the Cree land users who guided us on the field. We thank Amy McMackin, Constance Duffaud, and Alexandra Aymard for their contribution to this specific project, as well as Fanny Noisette, Bruno Cayouette, Yannick Grégo, Kaushik Gupta, Christian Boutot, Rémi Costanzo, Lou Richer, Manfred Desirer Neytem, Félis Lachapelle, Jessica Lambert Pineault, Rémi Amiraux, Laélien Bassi, Raphael Mabit, Michael Bianchi, Zélie Schuhmacher, Marie-Hélène Carignan, Valentin Gaillardon, Loïc Théberge Dallaire, Chloé Pelletier, and Marie-Claude Bourboin for their contribution to the field work. We are grateful to Claude Belzile for DOC analysis, Jean-François Hélie for the $\delta^{18}O$-H_2O analysis and Pascal Guillot for the CTD data processing and quality control. This work was funded by Niskamoon Corporation and by grants from the Natural Sciences and Engineering Research Council of Canada (NSERC). Partial funding was provided by the Fonds de recherche du Québec – Nature et technologies (FRQNT) through Québec-Océan and Northern Scientific Training Program of Polar Knowledge Canada. This project is a contribution to the larger Coastal Habitat Comprehensive Research Program aiming to understand changes in the coastal habitats of Eeyou Istchee (James Bay).

CONCLUSION GÉNÉRALE

Ce mémoire avait pour objectifs principaux 1) d'évaluer l'impact de la régulation du débit des rivières sur l'abondance et les caractéristiques chimiques de la CDOM terrestre déversée dans l'est de la baie James, 2) de caractériser la dynamique de mélange de la CDOM et sa potentielle variabilité saisonnière et interannuelle dans la baie, et 3) d'étudier la possibilité d'utiliser la CDOM comme indicateur du carbone organique dissous dans l'est de la baie James. Une analyse détaillée des données a montré que l'eau douce rejetée par la Grande Rivière, dont le débit est régulé, est fortement appauvrie en CDOM par rapport à celle des rivières non régulées de la côte est de la baie James. D'un point de vue qualitatif, le réservoir de CDOM de la Grande Rivière et celui des rivières non régulées ne sont que modérément différents en terme de poids moléculaire ($P = 0.6$) et d'aromaticité ($P = 0.008$), comme l'indiquent $S_{275\text{-}295}$ et $a^*_{CDOM}(254)$, respectivement. Les résultats de cette étude nous permettent de proposer l'hypothèse que cette divergence entre la quantité et la qualité proviendrait du temps de séjour plus long de l'eau dans les dix réservoirs du bassin versant de la Grande Rivière, permettant à la CDOM de subir des dégradations photochimiques et microbiennes plus importantes, qui consomment toutes deux de la CDOM, mais qui exercent chacune un effet opposé sur le poids moléculaire et l'aromaticité de la CDOM résiduelle. La fonctionnalité des ratios $S_{275\text{-}295}$ et $a^*_{CDOM}(254)$ pour déduire la nature et l'étendue de la transformation de la CDOM est donc limitée dans les milieux où les dégradations photochimiques et microbiennes sont tout aussi importantes pour modifier la qualité de la CDOM. La combinaison de la faible teneur en CDOM de la Grande Rivière et de son débit élevé en eau douce fait en sorte qu'une grande partie du nord de la baie James, et potentiellement une partie du sud de la baie d'Hudson, est beaucoup plus transparente à la lumière que si le débit de la Grande Rivière n'avait pas été régulé. La régulation de la Grande Rivière ne modifie donc pas seulement considérablement l'hydrodynamique et la répartition

de la salinité, mais peut également avoir un impact profond sur les propriétés optiques, les cycles biogéochimiques et l'écologie de la baie James.

Les différences de CDOM fluviale entre La Grande Rivière et les rivières non-régulées donnent lieu à des schémas de mélange distincts. La Grande Rivière est appauvrie en CDOM, tandis que les rivières non-régulées présentent des niveaux naturels de CDOM, reflétant ainsi les propriétés et concentrations qui sont mieux représentatives du bassin versant. Cette distinction offre une opportunité potentielle de les utiliser pour distinguer et tracer les masses d'eau douce provenant des deux systèmes dans l'est de la baie James. Le comportement de mélange très conservateur de la CDOM avec une saisonnalité très faible (zone influencée par la Grande Rivière) ou marginale (zone influencée par les rivières non régulées) distingue l'est de la baie James de nombreux autres systèmes nordiques influencés par des rivières caractérisées par une variabilité saisonnière prononcée de la dynamique de mélange de la CDOM.

La corrélation linéaire de premier ordre simple et robuste, entre le carbone organique dissous (DOC) et le $a_{CDOM}(440)$, associée à une faible variabilité spatio-temporelle, rend la télédétection plus fiable pour estimer la concentration en DOC en utilisant le $a_{CDOM}(440)$ comme proxy. Cette approche est d'autant plus avantageuse étant donné que la télédétection est une méthode potentiellement peu coûteuse et efficace, offrant une couverture spatiale et temporelle étendue. Ceci rendrait plus facilement accessibles des données sur les systèmes, qui pourraient être utilisées dans des recherches appliquées visant à mieux comprendre le système dans son ensemble. Les relations quantitatives identifiées entre $S_{275-295}$, $a^*_{CDOM}(254)$ et l'$a_{CDOM}(440)$, encore une fois largement indépendantes des saisons et des régions, permettent également d'évaluer potentiellement la qualité de la CDOM depuis l'espace. Ces résultats démontrent la faisabilité d'une surveillance synoptique et en temps réel de la dynamique et des caractéristiques de la matière organique dissoute dans l'est de la baie James et, éventuellement, dans l'ensemble de la baie James.

Cette étude nous a permis de mieux comprendre comment la régulation des cours d'eau peut affecter l'abondance et la qualité de la CDOM fluviale livrée aux zones de transition

terre-mer dans les régions nordiques, ainsi que les processus de mélange et les cycles biogéochimiques qui en découlent. Elle révèle la sensibilité saisonnière et interannuelle étonnamment faible de la dynamique de mélange de la CDOM dans l'est de la baie James et souligne les implications de cette stabilité temporelle pour l'évaluation par satellite en temps réel et à l'échelle de la baie de la dynamique de la matière organique dissoute et, plus généralement, des cycles biogéochimiques et de l'écologie liés à la matière organique dissoute.

Dans l'avenir, il serait intéressant d'étudier la dynamique de la CDOM dans les rivières qui coulent du côté occidental de la baie James, entre autres, la rivière Moose qui est régulée et la rivière Albany qui ne l'est pas, ainsi que celles du sud-ouest de la baie d'Hudson qui entre dans la baie James grâce à la circulation cyclonique. Puisque les feux de forêt sont susceptibles de s'intensifier avec le changement climatique, il serait également souhaitable d'étudier l'impact de ces feux sur la quantité et la qualité de la matière organique dissoute et particulaire dans les rivières se jetant dans la baie James et la baie d'Hudson. Enfin, il faut souligner l'importance de poursuivre les collaborations avec les communautés autochtones locales, pour répondre aux déficits des connaissances scientifiques régionales grâce à leur savoir traditionnel qui apporte une meilleure compréhension spatiotemporelle du territoire qu'ils ont habité et utilisé pendant des générations.

Bien que ce mémoire n'ait pas spécifiquement étudié l'impact de la présence de barrages et de réservoirs, les différences observées dans la CDOM fluviale entre la Grande Rivière et les rivières non-régulées suggèrent que leur présence pourrait altérer les propriétés qualitative et quantitative de la DOM et de la CDOM, influençant ainsi le cycle du carbone en plus du cycle hydrologique. Ces observations suscitent des réflexions intéressantes sur les facteurs qui pourraient influencer ce phénomène à l'échelle mondiale, notamment les caractéristiques géographiques, environnementales et structurelles des systèmes. Une meilleure compréhension de ce phénomène permettrait une évaluation plus précise de l'impact en termes de carbone que les barrages et réservoirs existants et futurs peuvent avoir sur les cycles du carbone régionales et globales.

ANNEXES

Informations supplémentaires de l’article

Tableau S1. Pearson's coefficient of correlation between different optical parameters of CDOM for the entire dataset reported in this study. SR = $S_{275-295}/S_{350-400}$.

	$a_{CDOM}(254)$	$a_{CDOM}(325)$	$a_{CDOM}(330)$	$a_{CDOM}(350)$	$a_{CDOM}(355)$	$a_{CDOM}(375)$	$a_{CDOM}(412)$	$a_{CDOM}(440)$	$a_{CDOM}(443)$	$a^*_{CDOM}(254)$	$S_{275-295}$	SR	$S_{300-650}$
$a_{CDOM}(325)$	0.998												
$a_{CDOM}(330)$	0.998	1.000											
$a_{CDOM}(350)$	0.997	1.000	1.000										
$a_{CDOM}(355)$	0.997	1.000	1.000	1.000									
$a_{CDOM}(375)$	0.997	0.999	1.000	1.000	1.000								
$a_{CDOM}(412)$	0.994	0.998	0.998	0.999	0.999	0.999							
$a_{CDOM}(440)$	0.993	0.997	0.997	0.998	0.998	0.999	1.000						
$a_{CDOM}(443)$	0.993	0.997	0.997	0.998	0.998	0.999	1.000	1.000					
$a^*_{CDOM}(254)$	0.679	0.677	0.677	0.675	0.675	0.675	0.674	0.676	0.676				
$S_{275-295}$	-0.813	-0.825	-0.826	-0.827	-0.828	-0.832	-0.839	-0.842	-0.842	-0.697			
SR	-0.801	-0.808	-0.809	-0.808	-0.808	-0.805	-0.801	-0.802	-0.802	-0.699	0.896		
$S_{300-650}$	-0.616	-0.633	-0.635	-0.640	-0.642	-0.648	-0.663	-0.670	-0.671	-0.532	0.860	0.725	
E2/E3	-0.753	-0.766	-0.767	-0.770	-0.772	-0.774	-0.782	-0.786	-0.786	-0.675	0.959	0.825	0.614

Tableau S2. Fitted parameters of the mixed models with sampling locations and years as random effects. The multiplication sign (×) denotes testing for interactions (i.e., with regions or seasons).

Region	Model	Parameter	Estimate	Standard error	*p*-value	Comment
All	$a_{CDOM}(440)$ *vs.* salinity × regions	Intercept south	7.64	0.14	3.0E-39	Relationships statistically different between regions
		Slope south	-0.28	0.01	1.3E-145	
		Intercept north	2.19	0.16	2.1E-32	
		Slope north	-0.05	0.01	1.4E-73	
All	$S_{275-295}$ *vs.* log($a_{CDOM}(440)$) × regions	Intercept south	16.68	0.18	8.2E-09	Relationships not statistically different between regions
		Slope south	-1.89	0.04	4.0E-212	
		Intercept north	16.49	0.06	1.4E-03	
		Slope north	-1.85	0.08	6.2E-01	
All	$a^*_{CDOM}(254)$ *vs.* log($a_{CDOM}(440)$) × regions	Intercept south	7.21	0.15	1.3E-13	Relationships statistically different between regions
		Slope south	4.11	0.14	< 2E-16	
		Intercept north	7.05	0.13	2.4E-01	
		Slope north	4.87	0.28	7.8E-03	
North	$a_{CDOM}(440)$ *vs.* salinity × seasons	Intercept spring	2.09	0.11	7.3E-39	Relationships not statistically different across seasons
		Slope spring	-0.04	0.01	8.4E-10	
		Intercept summer	2.28	0.13	1.5E-01	
		Intercept fall	2.10	0.21	9.8E-01	
		Intercept Winter	2.26	0.12	1.9E-01	
		Slope summer	-0.05	0.01	1.7E-01	
		Slope fall	-0.05	0.01	5.3E-01	
		Slope winter	-0.06	0.01	5.1E-02	
South	$a_{CDOM}(440)$ *vs.* salinity × seasons	Intercept spring	7.42	0.33	1.4E-20	Relationships statistically different across seasons
		Slope spring	-0.28	0.02	6.4E-37	
		Intercept summer	8.21	0.35	2.6E-02	
		Intercept fall	12.24	0.81	9.2E-09	
		Intercept winter	6.79	0.39	1.1E-01	
		Slope summer	-0.33	0.02	1.1E-02	
		Slope fall	-0.52	0.04	3.6E-08	
		Slope winter	-0.22	0.02	1.2E-02	

Tableeau S2 (continued)

All	δO^{18}-H_2O *vs.* salinity × seasons	Intercept spring	-13.96	0.15	9.6E-49	Relationships not statistically different across seasons
		Slope spring	0.37	0.01	2.1E-240	
		Intercept summer	-14.00	0.10	7.0E-01	
		Intercept fall	-13.70	0.19	1.7E-01	
		Intercept winter	-13.93	0.10	7.8E-01	
		Slope summer	0.38	0.01	1.0E-01	
		Slope fall	0.36	0.01	3.2E-01	
		Slope winter	0.36	0.01	5.6E-01	
All	$S_{275\text{-}295}$ *vs.* log(a_{CDOM}(440)) × seasons	Intercept spring	16.78	0.11	7.6E-24	Relationships statistically different for some seasons
		Slope spring	-2.04	0.07	1.3E-131	
		Intercept summer	17.06	0.07	8.0E-05	
		Intercept fall	17.08	0.09	1.1E-03	
		Intercept winter	16.42	0.08	8.5E-06	
		Slope summer	-2.07	0.07	6.6E-01	
		Slope fall	-2.28	0.13	6.4E-02	
		Slope winter	-1.65	0.08	3.0E-06	
All	a^*_{CDOM}(254) *vs.* log(a_{CDOM}(440)) ×seasons	Intercept spring	6.43	0.15	1.8E-39	Relationships statistically different for some seasons
		Slope spring	5.50	0.32	1.2E-53	
		Intercept summer	7.15	0.13	1.2E-08	
		Intercept fall	6.97	0.15	2.1E-04	
		Intercept winter	7.46	0.13	5.4E-14	
		Slope summer	4.48	0.35	3.6E-03	
		Slope fall	4.03	0.48	2.1E-03	
		Slope winter	3.62	0.36	1.7E-07	
All	DOC *vs.* a_{CDOM}(440) × seasons	Intercept spring	2.17	0.14	6.7E-25	Relationships statistically different for some seasons
		Slope spring	1.1	0.04	1.2E-118	
		Intercept summer	2.04	0.10	2.1E-01	
		Intercept fall	2.13	0.12	7.7E-01	
		Intercept winter	1.56	0.11	1.9E-08	
		Slope summer	1.11	0.04	8.9E-01	
		Slope fall	1.08	0.05	5.6E-01	
		Slope winter	1.27	0.04	2.1E-05	

Tableau S3. Post-hoc Tukey test of the mixed model with statistically significant relationships across factors (see Table S1). The multiplication sign (×) denotes testing for interactions (i.e., with regions or seasons).

Model	Contrast	*p*-value
$a_{CDOM}(440)$ *vs.* salinity × seasons (south)	Spring - Summer	0.669
	Spring - Fall	0.018
	Spring - Winter	0.168
	Summer - Fall	0.001
	Summer - Winter	< 0.0001
	Fall - Winter	0.461
$S_{275-295}$ *vs.* log($a_{CDOM}(440)$) × seasons	Spring - Summer	<0.0001
	Spring - Fall	0.687
	Spring - Winter	0.955
	Summer - Fall	0.239
	Summer - Winter	< 0.0001
	Fall - Winter	0.510
$a^*_{CDOM}(254)$ *vs.* log($a_{CDOM}(440)$) × seasons	Spring - Summer	< 0.0001
	Spring - Fall	0.994
	Spring - Winter	< 0.0001
	Summer - Fall	0.023
	Summer - Winter	1.000
	Fall - Winter	0.026
DOC *vs.* $a_{CDOM}(440)$ × seasons	Fall - Spring	0.540
	Fall - Summer	0.996
	Fall - Winter	0.334
	Spring - Summer	0.179
	Spring - Winter	0.001
	Summer - Winter	0.050

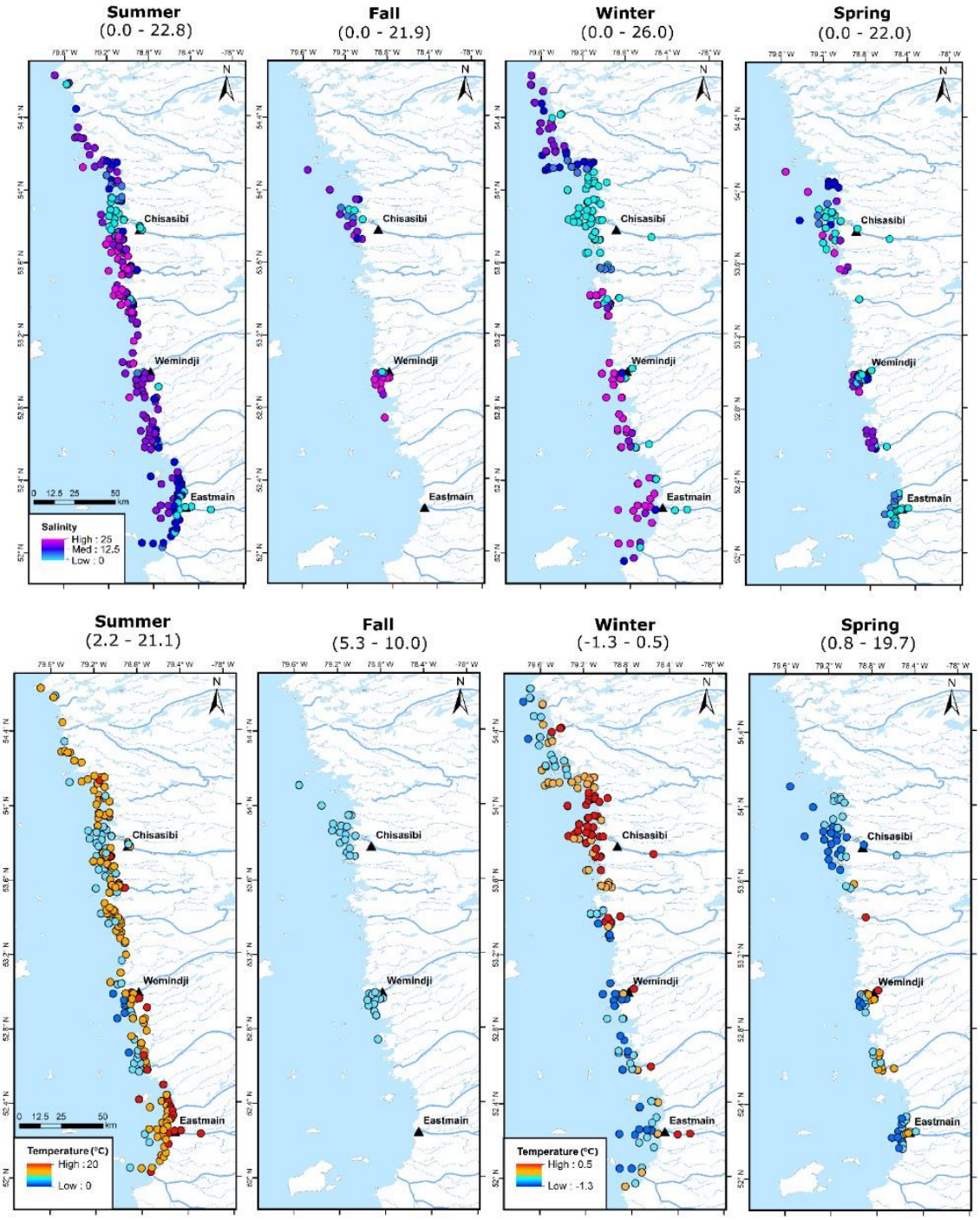

Figure S1. Surface salinity (top) and temperature (bottom) along the eastern James Bay coast during different seasons from 2018 to 2021. The winter temperature map has its own scale. Mean values and the ranges (in parenthesis) are indicated above the map.

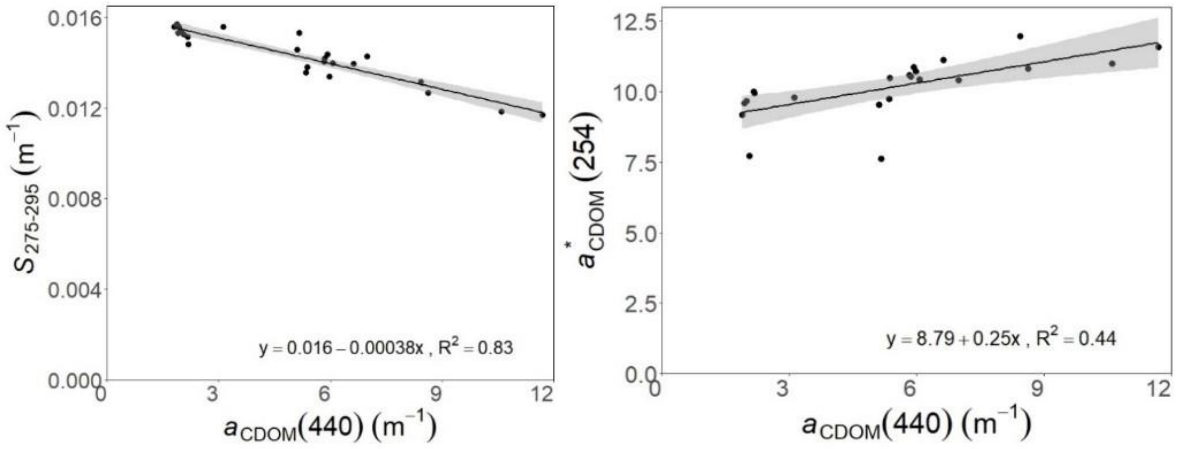

Figure S2. Figure S2. Relationships between $S_{275-295}$ and $a_{CDOM}(440)$ (left) and between $a^*_{CDOM}(254)$ and $a_{CDOM}(440)$ (right) for the river endmembers (Table 1 in the main text). The solid line represents the linear fit of the composite data (the LGR and URRs combined) and the shaded area denotes the 95% confidence interval.

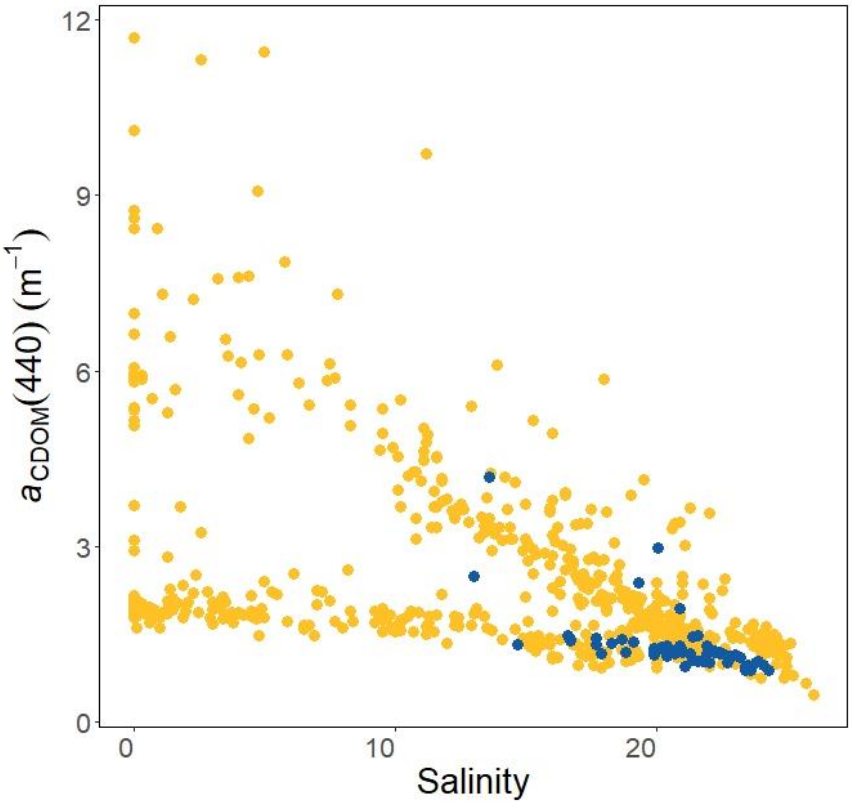

Figure S3. Scatter plot of $a_{CDOM}(440)$ against salinity for all sampling campaigns combined. Yellow dots denote surface samples and blue dots represent under-pycnocline samples.

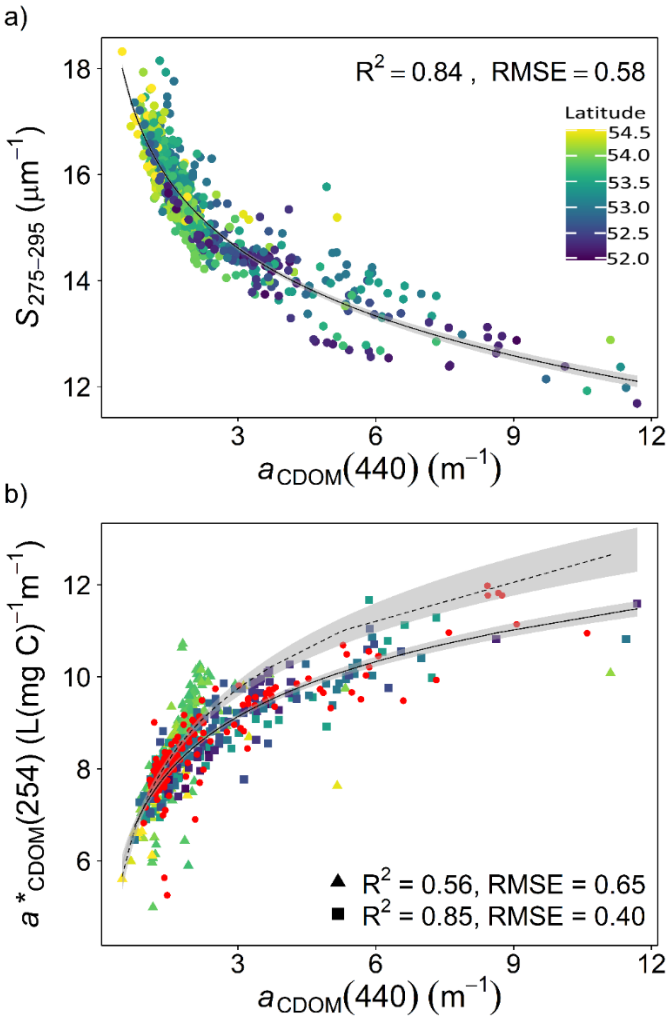

Figure S4. Scatter plots of $S_{275\text{-}295}$ (**a**) and $a^*_{CDOM}(254)$ (**b**) against $a_{CDOM}(440)$ with color scale denoting latitude (°N). Triangles in the lower panel stands for data collected from the LGR-influenced area and squares (non-red colors) for data from the URRs-influenced area. Solid black line in panel **a** represents the fit of the composite data to the simple logarithmic function. Solid and dashed black lines in panel **b** represent the fits to the simple logarithmic function for the URRs- and LGR-influenced area, respectively. Shaded areas represent the 95% confidence interval. Red squares in panel **b** represent the stations directly south of the LGR excluded from the fitting. The fits for $a^*_{CDOM}(254)$ are significantly different (p = 0.013) at α = 0.05 between the LGR- and URRs-influenced area. The fitted lines for $S_{275\text{-}295}$ for the two individual areas are not shown because the fits are not significantly different (p = 0.979). The fitted equations for both panels **a** and **b** can be found in Table S2. RMSE: root mean square error.

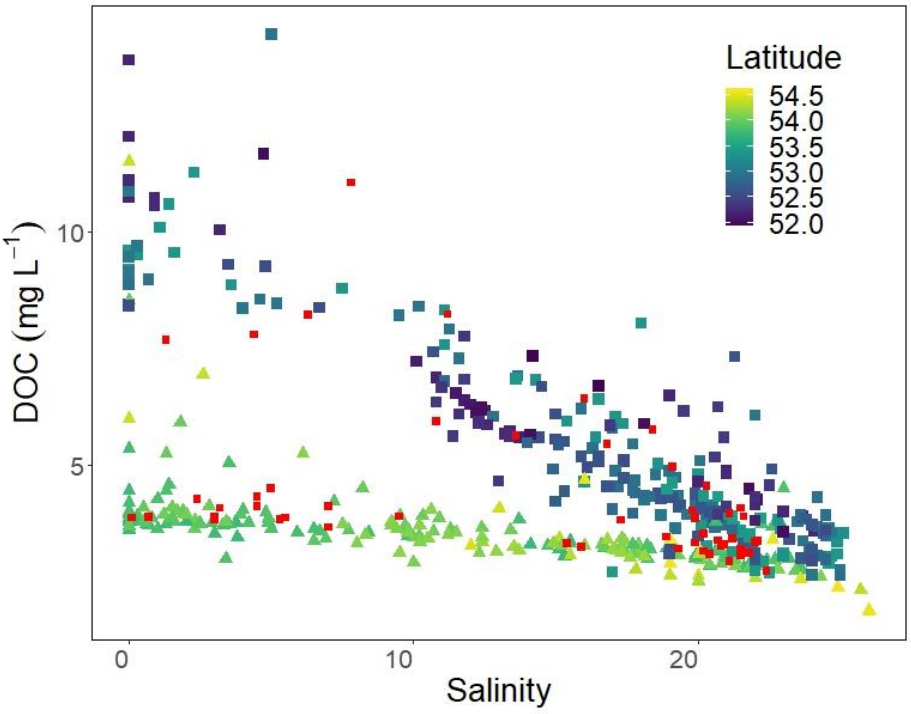

Figure S5. Scatter plots of DOC against salinity for all sampling campaigns combined. Triangles stand for the sampling stations of the La Grande River plume and north of the La Grande River, squares (non-red colors) for the stations south of the La Grande River, and red squares for the stations directly south of the La Grande River. The color scale represents the latitude (°N).

RÉFÉRENCES BIBLIOGRAPHIQUES

Aarup, T., Holt, N. et Højerslev, N.K. (1996). Optical measurements in the North Sea–Baltic Sea transition zone. II. Water mass classification along the Jutland west coast from salinity and spectral irradiance measurements, *Continental Shelf Research*, *16*, 1343–1353.

Aiken, G.R., Hsu-Kim, H. et Ryan, J.N. (2011). Influence of Dissolved Organic Matter on the Environmental Fate of Metals, Nanoparticles, and Colloids, *Environmental Science & Technology*, *45*(8), 3196–3201.

Altare, N. et Vione, D. (2023). Photochemical Implications of Changes in the Spectral Properties of Chromophoric Dissolved Organic Matter: A Model Assessment for Surface Waters, *Molecules*, *28*(6), 2664.

Asmala, E., Stedmon, C.A. et Thomas, D.N. (2012). Linking CDOM spectral absorption to dissolved organic carbon concentrations and loadings in boreal estuaries, *Estuarine, Coastal and Shelf Science*, *111*, 107-117.

Asmala, E., Bowers, D.G., Autio, R., Kaartokallio, H. et Thomas, D.N. (2014). Qualitative changes of riverine dissolved organic matter at low salinities due to flocculation, *Journal of Geophysical Research: Biogeosciences*, *119*, 1919-1933.

Asmala, E., Kaartokallio, H., Carstensen, J. et Thomas, D.N. (2016). Variation in riverine inputs affect dissolved organic matter characteristics throughout the estuarine gradient, *Frontiers in Marine Science*, *2*, 125.

Aurin, D., Mannino, A. et Franz, B. (2013). Spatially resolving ocean color and sediment dispersion in river plumes, coastal systems, and continental shelf waters, *Remote Sensing of Environment*, *137*, 212-225.

Babin, M., Stramski, D., Ferrari, G.M., Claustre, H., Bricaud, A., Obolensky, G. et Hoepffner, N. (2003). Variations in the light absorption coefficients of phytoplankton, nonalgal particles, and dissolved organic matter in coastal waters around Europe, *Journal of Geophysical Research: Oceans*, *108*(C7), 3211.

Barbecot, F., Guillon, S., Pili, E., Larocque, M., Gibert-Brunet, E., Hélie, J. F., Noret, A., Plain, C., Schneider, V., Mattei, A. et Meyzonnat, G. (2018). Using water stable isotopes in the unsaturated zone to quantify recharge in two contrasted infiltration regimes, *Vadose Zone Journal*, *17*, 170170.

Barsugli, J. J., Whitaker, J. S., Loughe, A. F., Sardeshmukh, P. D. et Toth, Z. (1999). The effect of the 1997/98 El Niño on individual large-scale weather events, *Bulletin of the American Meteorological Society*, *80*(7), 1399–1411.

Bates, D., Mächler, M., Bolker, B. et Walker, S. (2014). Fitting Linear Mixed-Effects Models Using lme4. ArXiv e-prints. arXiv:1406. 10.18637/jss.v067.i01.

Battin, T. J., Kaplan, L. A., Findlay, S., Hopkinson, C.S., Marti, E., Packman, A.I., Newbold, J.D. et Sabater, F. (2008). Biophysical controls on organic carbon fluxes in fluvial networks, *Nature Geoscience*, *1*, 95-100.

Bauer J.E. et Bianchi T.S. (2011). Dissolved Organic Carbon Cycling and Transformation. Dans: Wolanski, E. et McLusky, D.S. (eds.) Treatise on Estuarine and Coastal Science, Volume 5, Academic Press, Waltham, MA, USA, 7–67.

Bélanger, S., Babin, M. et Larouche, P. (2008). An empirical ocean color algorithm for estimating the contribution of chromophoric dissolved organic matter to total light absorption in optically complex waters, *Journal of Geophysical Research: Oceans*, *113*(C4), C04027.

Blanchet, C.C., Arzel, C., Davranche, A., Kahilainen, K.K., Secondi, J., Taipale, S., Lindberg, H., Loehr, J., Manninen-Johansen, S., Sundell, J., Maanan, M. et Nummi, P. (2022). Ecology and extent of freshwater browning - What we know and what should be studied next in the context of global change, *Science of the Total Environment*, *812*, 152420.

Blough, N.V. et Del Vecchio, R. (2002). Chromophoric DOM in the Coastal Environment. Dans: Hansell, D.A. and Carlson, C.A., Eds., Biogeochemistry of Marine Dissolved Organic Matter, Academic Press, San Diego, CA, USA, 509-546.

Blough, N.V. et R. G. Zepp (1995), Reactive oxygen species in natural waters. Dans: Liebman, J.F. (eds) Active Oxygen in Chemistry, Chapman and Hall, New York, NY, USA, 280–333.

Bricaud, A., Morel, A. et Prieur, L. (1981). Absorption by dissolved organic matter of the sea (yellow substance) in the UV and visible domains, *Limnology Oceanography*, *26*, 43-53.

Brogi, S.R., Ha, S.Y., Kim, K., Derrien, M., Lee, Y.K. et Hur, J. (2018). Optical and molecular characterization of dissolved organic matter (DOM) in the Arctic ice core and the underlying seawater (Cambridge Bay, Canada): Implication for increased autochthonous DOM during ice melting, *Science of the Total Environment*, *627*, 802-811.

Coble, P.G. (2007). Marine optical biogeochemistry: the chemistry of ocean color, *Chemical Reviews*, *107*, 402-418.

De Haan, H. et De Boer, T. (1987). Applicability of light absorbance and fluorescence as measures of concentration and molecular size of dissolved organic carbon in humic Lake Tjeukemeer, *Water Research*, *21*, 731-734.

de Melo, M.L., Gérardin, M.-L., Fink-Mercier, C. et del Giorgio, P.A. (2022). Patterns in riverine carbon, nutrient and suspended solids export to the Eastern James Bay: links to climate, hydrology and landscape, *Biogeochemistry*, *161*, 291–314.

Del Vecchio, R., et Blough, N.V. (2004). Spatial and seasonal distribution of chromophoric dissolved organic matter and dissolved organic carbon in the Middle Atlantic Bight, *Marine Chemistry*, *89*, 169-187.

Denis, M., Jeanneau, L., Pierson-Wickman, A. C., Humbert, G., Petitjean, P., Jaffrézic, A., et Gruau, G. (2017). A comparative study on the pore-size and filter type effect on the molecular composition of soil and stream dissolved organic matter, *Organic Geochemistry*, *110*, 36-44.

Déry, S.J., Stadnyk, T.A., MacDonald, M.K. et Gauli-Sharma, B. (2016). Recent trends and variability in river discharge across northern Canada, *Hydrology and Earth System Sciences*, *20*, 4801-4818.

Déry, S.J., Stieglitz, M., McKenna, E.C. et Wood, E.F. (2005). Characteristics and trends of river discharge into Hudson, James, and Ungava Bays, 1964–2000, *Journal of Climate*, *18*, 2540-2557.

Dionne, JC. (1978). Formes et phénomènes périglaciaires en Jamésie, Québec subarctique, *Géographie physique et Quaternaire*, *32*, 187–247.

El-Sabh, M.I. et Koutitonsky, V.G. (1977). An oceanographic study of James Bay before the completion of the La Grande hydroelectric complex, *Arctic*, *30*, 169-186.

Erni, S., Arseneault, D., Parisien, M.-A. et Bégin, Y. (2016). Spatial and temporal dimensions of fire activity in the fire-prone eastern Canadian taiga, *Global Change Biology*, *23*(3), 1152-1166.

Fichot, C.G. et Benner, R. (2011). A novel method to estimate DOC concentrations from CDOM absorption coefficients in coastal waters, *Geophysical research letters*, *38*, L03610.

Fichot, C.G. et Benner, R. (2012). The spectral slope coefficient of chromophoric dissolved organic matter (S275–295) as a tracer of terrigenous dissolved organic carbon in river-influenced ocean margins, *Limnol. Oceanogr.*, *57(5)*, 1453–1466.

Fink-Mercier, C., Lapierre, J.-F., Amyot, M. et del Giorgio, P. A. (2022). Concentrations and yields of total Hg and MeHg in large boreal rivers linked to water and wetland coverage in the watersheds, *Journal of Geophysical Research: Biogeosciences*, *127*, e2022JG006892.

Fox-Kemper, B., Hewitt, H.T., Xiao, C., Aðalgeirsdóttir, G., Drijfhout, S.S., Edwards, T.L., Golledge, N.R., Hemer, M., Kopp, R.E., Krinner, G., Mix, A., Notz, D., Nowicki, S., Nurhati, I.S., Ruiz, L., Sallée, J.-B., Slangen, A.B.A. et Yu, Y. (2021) Ocean, Cryosphere and Sea Level Change. Dans: Masson-Delmotte, V., Zhai, P., A., Pirani, Connors, S.L., Péan, C., Berger, S., Caud, N., Chen, Y., Goldfarb, L., Gomis, M.I., Huang, M., Leitzell, K., Lonnoy, E., Matthews, J.B.R., Maycock, T.K., Waterfield, T., Yelekçi, O., Yu, R. et Zhou, B. (Eds.) Climate Change 2021: The Physical Science Basis. Contribution of Working Group I to the Sixth Assessment Report of the Intergovernmental Panel on Climate Change, Cambridge University Press Cambridge, United Kingdom and New York, NY, USA, 1211–1362.

Galbraith, P.S. et Larouche, P. (2011). Sea-surface temperature in Hudson Bay and Hudson Strait in relation to air temperature and ice cover breakup, 1985-2009, *Journal of Marine Systems*, *88*, 463-475.

Goncalves-Araujo, R., Rabe, B., Peeken, I. et Bracher, A. (2018). High colored dissolved organic matter (CDOM) absorption in surface waters of the central-eastern Arctic Ocean: Implications for biogeochemistry and ocean color algorithms, *PLoS One*, *13*, e0190838.

Granskog, M.A. (2012). Changes in spectral slopes of colored dissolved organic matter absorption with mixing and removal in a terrestrially dominated marine system (Hudson Bay, Canada), *Marine Chemistry*, *134*, 10-17.

Granskog, M.A., Kuzyk, Z.Z.A., Azetsu-Scott, K. et Macdonald, R.W. (2011). Distributions of runoff, sea-ice melt and brine using $\delta^{18}O$ and salinity data—A new view on freshwater cycling in Hudson Bay, *Journal of Marine Systems*, *88*, 362-374.

Granskog, M.A., Macdonald, R.W., Kuzyk, Z.Z.A., Senneville, S., Mundy, C.J., Barber, D.G., Stern, G.A. et Saucier, F. (2009). Coastal conduit in southwestern Hudson Bay (Canada) in summer: Rapid transit of freshwater and significant loss of colored dissolved organic matter, *Journal of Geophysical Research: Oceans*, *114*, C08012.

Granskog, M.A., Macdonald, R.W., Mundy, C.-J. et Barber, D.G. (2007). Distribution, characteristics and potential impacts of chromophoric dissolved organic matter (CDOM) in Hudson Strait and Hudson Bay, Canada, *Continental Shelf Research*, *27*, 2032-2050.

Granskog, M. A., Pavlov, A. K., Sagan, S., Kowalczuk, P., Raczkowska, A. et Stedmon, C. A. (2015). Effect of sea-ice melt on inherent optical properties and vertical distribution of solar radiant heating in Arctic surface waters, *Journal of Geophysical Research: Oceans, 10*, 7029-7036.

Gregor, J.E., Nokes, C.J. et Fenton, E. (1997). Optimising natural organic matter removal from low turbidity waters by controlled pH adjustment of aluminium coagulation, Water Research, 31(12), 2949–2958.

Griffin, C., McClelland, J., Frey, K., Fiske, G. et Holmes, R. (2018). Quantifying CDOM and DOC in major Arctic rivers during ice-free conditions using Landsat TM and ETM+ data, *Remote Sensing of Environment*, *209*, 395-409.

Guay, C., Minville, M. et Braun, M. (2015). A global portrait of hydrological changes at the 2050 horizon for the province of Québec, *Canadian Water Resources Journal/Revue canadienne des ressources hydriques*, *40*, 285-302.

Guéguen, C., Granskog, M., McCullough, G. et Barber, D. (2011). Characterisation of colored dissolved organic matter in Hudson Bay and Hudson Strait using parallel factor analysis, *Journal of Marine Systems*, *88*, 423-433.

Guéguen, C., Mokhtar, M., Perroud, A., McCullough, G. et Papakyriakou, T. (2016). Mixing and photoreactivity of dissolved organic matter in the Nelson/Hayes estuarine system (Hudson Bay, Canada), *Journal of Marine Systems*, *161*, 42-48.

Guzzi, A. (2022). Freshwater and nutrient distributions in contrasting coastal domains of Hudson Bay and James Bay, Master's thesis, University of Manitoba, Winnipeg, Canada.

Häder, D.-P., Helbling, E.W., Williamson, C.E et Worrest R.C. (2011). Effects of UV radiation on aquatic ecosystems and interactions with climate change, Photochemical & Photobiological. Sciences, 10, 242–260.

Hansell, D.A. et Carlson, C.A., 2002. Biogeochemistry of Marine Dissolved Organic Matter, Academic Press, San Diego, CA, USA, 774 p.

Hansen, A.M., Kraus, T.E., Pellerin, B.A., Fleck, J.A., Downing, B.D. et Bergamaschi, B.A. (2016). Optical properties of dissolved organic matter (DOM): Effects of biological and photolytic degradation, *Limnology and Oceanography*, *61*, 1015-1032.

Harvey, E.T., Kratzer, S. et Andersson, A. (2015). Relationships between colored dissolved organic matter and dissolved organic carbon in different coastal gradients of the Baltic Sea, *Ambio, 44*, 392-401.

Helms, J.R., Stubbins, A., Ritchie, J.D., Minor, E.C., Kieber, D.J. et Mopper, K. (2008). Absorption spectral slopes and slope ratios as indicators of molecular weight, source, and photobleaching of chromophoric dissolved organic matter, *Limnology and Oceanography, 53*, 955-969.

Hernández-Henríquez, M. A., Mlynowski, T. J. et Déry, S. J. (2010). Reconstructing the Natural Streamflow of a Regulated River: A Case Study of La Grande Rivière, Québec, Canada. *Canadian Water Resources Journal/Revue canadienne des ressources hydriques, 35*(3), 301-316.

IOCCG. (2021). Ocean Optics and Biogeochemistry Protocols for Satellite Ocean Colour Sensor Validation, Volume 6: Particulate Organic Matter Sampling and Measurement Protocols: Consensus Towards Future Ocean Color Missions, Dans: Chaves, J. E., Cetinić, I., Dall'Olmo, G., Estapa, M., Gardner, W., Goñi, M., Graff, J. R., Hernes, P., Lam, P.J., Liu, Z., Lomas, M. W., Mannino, A., Novak, M. G., Turnewitsch, R., Werdell, P. J., Westberry, T. K. (Eds). International Ocean-Colour Coordinating Group (IOCCG) Protocol Series, Volume 6, Dartmouth, NS, Canada, 54 p.

Jia, G., Shevliakova, E., Artaxo, P., De Noblet-Ducoudré, N., Houghton, R., House, J., Kitajima, K., Lennard, C., Popp, A., Sirin, A., Sukumar, R. et Verchot, L. (2019) Land–climate interactions. Dans: Shukla, P.R., Skea, J., Calvo Buendia, E., Masson-Delmotte, V., Pörtner, H.-O., Roberts, D.C., Zhai, P., Slade, R., Connors, S., van Diemen, R., Ferrat, M., Haughey, E., Luz, S., Neogi, S., Pathak, M., Petzold, J., J. Portugal Pereira, P. Vyas, E. Huntley, K. Kissick, M, Belkacemi, J. Malley, (eds.)Climate Change and Land: an IPCC special report on climate change, desertification, land degradation, sustainable land management, food security, and greenhouse gas fluxes in terrestrial ecosystems. https://doi.org/10.1017/9781009157988.004

Johnston, S.E., Carey, J.C., Kellerman, A., Podgorski, D.C., Gewirtzman, J. et Spencer, R.G. (2021). Controls on riverine dissolved organic matter composition across an Arctic-boreal latitudinal gradient, *Journal of Geophysical Research: Biogeosciences*, *126*, e2020JG005988.

Jørgensen, L., Stedmon, C.A., Kaartokallio, H., Middelboe, M. et Thomas, D.N. (2015). Changes in the composition and bioavailability of dissolved organic matter during sea ice formation, *Limnology and Oceanography*, *60*, 817-830.

Juhls, B., Stedmon, C.A., Morgenstern, A., Meyer, H., Hölemann, J., Heim, B., Povazhnyi, V. et Overduin, P.P. (2020). Identifying drivers of seasonality in Lena River biogeochemistry and dissolved organic matter fluxes, *Frontiers in Environmental Science*, *8*, 53.

Kaufman, D.S., Schneider, D.P., McKay, N.P., Ammann, C.M., Bradley, R.S., Briffa, K.R., Miller, G.H., Otto-Bliesner, B.L., Overpeck, J.T., Vinther, B.M., Abbott, M., Axford, Y., Bird, B., Birks, H., Bjune, A., Briner, J., Cook, T., Chipman, M. Francus, P. et Thomas, E. (2009), Recent warming reverses long-term arctic cooling. *Science*, *325*, 1236-1239.

Kragh, T., Sand-Jensen, K., Kristensen, E., Pedersen, O. et Madsen-Østerbye, M. (2022). Removal of chromophoric dissolved organic matter under combined photochemical and microbial degradation as a response to different irradiation intensities, *Journal of Environmental Sciences*, *118*, 76-86.

Kuznetsova, A., Brockhoff, P.B. et Christensen, R.H.B. (2015). Package 'lmertest'. R package version 2(0), 734.

Lalumière, R. et Lemieux, C. (2002). Suivi environnemental des projets La Grande-2-A et La Grande-1. La zostère marine de la côte nord-est de la baie James. Rapport synthèse pour la période 1988-2000. Rapport du Groupe conseil GENIVAR inc. pour la Direction Barrages et Environnement, Hydro-Québec Production, QC, Canada, 92 p.

Landy, J.C., Ehn, J.K., Babb, D.G., Thériault, N. et Barber, D.G. (2017). Sea ice thickness in the Eastern Canadian Arctic: Hudson Bay Complex & Baffin Bay, *Remote Sensing of Environment*, *200*, 281-294.

LeGrande, A.N., et G.A. Schmidt, (2006). Global gridded data set of the oxygen isotopic composition in seawater, *Geophysical Research Letters*, *33*, L12604.

Lesser, M.P. (2006). OXIDATIVE STRESS IN MARINE ENVIRONMENTS: Biochemistry and Physiological Ecology, *Annual Review of Physiology*, *68*(1), 253–278.

Li, Y., Song, G., Massicotte, P., Yang, F., Li, R. et Xie, H. (2019). Distribution, seasonality, and fluxes of dissolved organic matter in the Pearl River (Zhujiang) estuary, China, *Biogeosciences*, *16*, 2751-2770.

Logozzo, L., Tzortziou, M., Neale, P. et Clark, J.B. (2021). Photochemical and microbial degradation of chromophoric dissolved organic matter exported from tidal marshes, *Journal of Geophysical Research: Biogeosciences*, *126*, e2020JG005744.

Lou, T. et Xie, H. (2006). Photochemical alteration of the molecular weight of dissolved organic matter, *Chemosphere*, *65*(11), 2333-2342.

Mabit, R., Bélanger, S., Araújo, C.A. et Singh, R.K. (2022). Empirical remote sensing algorithms to retrieve SPM and CDOM in Québec coastal waters, *Frontiers in Remote Sensing*, *3*, 834908.

Markager, S., Stedmon, C.A. et Søndergaard, M. (2011). Seasonal dynamics and conservative mixing of dissolved organic matter in the temperate eutrophic estuary Horsens Fjord, *Estuarine, Coastal and Shelf Science*, *92*, 376-388.

Massicotte, P., Asmala, E., Stedmon, C. et Markager, S. (2017). Global distribution of dissolved organic matter along the aquatic continuum: Across rivers, lakes and oceans, *Science of the Total Environment*, *609*, 180-191.

McClelland, J.W., Holmes, R.M., Dunton, K.H. et Macdonald, R.W. (2012). The Arctic Ocean estuary, *Estuaries and Coasts*, *35*, 353-368.

Mei, Z.-P., Saucier, F.J., Le Fouest, V., Zakardjian, B., Sennville, S., Xie, H. et Starr, M., (2010). Modeling the timing of spring phytoplankton bloom and biological production of the Gulf of St. Lawrence (Canada): Effects of colored dissolved organic matter and temperature, *Contnental Shelf Research*, *30*, 2027–2042.

Meilleur, C., Kamula, M., Kuzyk, Z. et Guéguen, C. (2023). Insights into surface circulation and mixing in James Bay and Hudson Bay from dissolved organic matter optical properties, *Journal of Marine Systems*, *238*, 103841.

Mopper, K., et D. J. Kieber (2002), The photochemistry and cycling of carbon, sulfur, nitrogen and phosphorus, Dans: Hansell, D.A. et Carlson, C.A., Eds., Biogeochemistry of Marine Dissolved Organic Matter, Academic Press, San Diego, CA, USA, 455–507.

Mopper, K., Kieber, D.J. et Stubbins, A., (2015). Marine photochemistry of organic matter: processes and impacts, Dans: Hansell, D.A. et Carlson, C.A., 2nd Eds., Biogeochemistry of marine dissolved organic matter, Academic Press, San Diego, CA, USA, 389-450.

Müller, S., Vähätalo, A.V., Stedmon, C.A., Granskog, M.A., Norman, L., Aslam, S.N., Underwood, G.J.C., Dieckmann, G.S. et Thomas, D.N. (2013). Selective incorporation of dissolved organic matter (DOM) during sea ice formation, *Marine Chemistry, 155*, 148-157.

Mundy, C.J., Gosselin, M. Starr, M. et Michel, C. (2010). Riverine export and the effects of circulation on dissolved organic carbon in the Hudson Bay system, Canada, *Limnology and Oceanography*, *55*(1), 315-323.

Nelson, N. et Siegel, D. (2002). Chromophoric DOM in the Open Ocean. Dans: Hansell, D.A. et Carlson, C.A., Eds., Biogeochemistry of Marine Dissolved Organic Matter, Academic Press, San Diego, CA, USA, 547–578.

Nelson, N. B., Dx Siegel, et Michaels, A. P. (1998). Seasonal dynamics of colored dissolved material in the Sargasso Sea, *Deep-Sea Research Part I: Oceanographic Research Papers*, *45*(6), 931-957.

Nelson, N.B., Siegel, D.A., Carlson, C.A. et Swan, C.M. (2010). Tracing global biogeochemical cycles and meridional overturning circulation using chromophoric dissolved organic matter, *Geophysical Research Letters*, *37*(3), L03610.

Norman, L., Thomas, D. N., Stedmon, C. A., Granskog, M. A., Papadimitriou, S., Krapp, R. H., Meiners, K. M., Lannuzel, D., van der Merwe, P., & Dieckmann, G.S. (2011). The characteristics of dissolved organic matter (DOM) and chromophoric dissolved organic matter (CDOM) in Antarctic Sea ice, *Deep Sea Research Part II: Topical Studies in Oceanography*, *58*(9-10), 1075-1091.

Osburn, C.L., Boyd, T.J., Montgomery, M.T., Bianchi, T.S., Coffin, R.B. et Paerl, H.W. (2016). Optical proxies for terrestrial dissolved organic matter in estuaries and coastal waters, *Frontiers in Marine Science*, *2*, 127.

Östlund, H. et Hut, G., 1984. Arctic Ocean water mass balance from isotope data, *Journal of Geophysical Research, 89 (C4)*, 6373–6381.

Peck, C.J., Kuzyk, Z.Z. A., Heath, J.P., Lameboy, J. et Ehn, J.K. (2022). Under-ice hydrography of the La Grande River plume in relation to a ten-fold increase in wintertime discharge, *Journal of Geophysical Research: Oceans*, *127*, e2021JC018341.

Pegau, W.S., Gray, D. et Zaneveld, J.R.V. (1997). Absorption and attenuation of visible and near-infrared light in water: dependence on temperature and salinity, *Applied Optics*, *36*, 6035-6046.

Pohl, S. Marsh, P. et Bonsal, B.R. (2007). Modeling the impact of climate change on runoff and annual of an arctic headwater basin, *Arctic*, *60*(2), 173-186.

Prinsenberg, S.J. (1980). Man-made changes in the freshwater input rates of Hudson and James Bays, *Canadian Journal of Fisheries and Aquatic Sciences*, *37*, 1101-1110.

Prinsenberg, S. (1986). The circulation pattern and current structure of Hudson Bay, *Elsevier Oceanography Series*, *44*, 187-204.

Prinsenberg, S. (1988). Ice-cover and ice-ridge contributions to the freshwater contents of Hudson Bay and Foxe Basin, *Arctic*, *41*, 6-11.

Roberts, C. D., LeGrande, A. N. et Tripati, A. K. (2011). Sensitivity of seawater oxygen isotopes to climatic and tectonic boundary conditions in an early Paleogene simulation with GISS ModelE-R, *Paleoceanography*, *26(4)*, PA4203.

Rohling E.J. (2013). Oxygen isotope composition of seawater, 2nd Edition. In: Elias S.A. (ed.) The Encyclopedia of Quaternary Science, Elsevier, Amsterdam, Pays-Bas, 915-922.

Roy, D. et Messier, D. (1989). A review of the effects of water transfers in the La Grande hydroelectric complex (Quebec, Canada), *Regulated Rivers: Research & Management*, *4*, 299-316.

Saucier, F.J. et Dionne, J. (1998). A 3-D coupled ice-ocean model applied to Hudson Bay, Canada: The seasonal cycle and time-dependent climate response to atmospheric forcing and runoff, *Journal of Geophysical Research-Oceans, 103*(C12), 27689–27705.

Schetagne, R, Therrien, J. et Lalumière, R. (2002). Suivi environnemental du complexe La Grande. Évolution des teneurs en mercure dans les poissons. Rapport synthèse 1978-2000. Rapport du Groupe GENIVAR inc. pour la Direction Barrages et Environnement, Hydro-Québec Production, Québec, Canada, 193 p.

Senneville, S. et St-Onge-Drouin, S. (2013). Étude de la variation des glaces dans le système couplé océan-glace de mer de la baie d'Hudson. Rapport final présenté au ministère des Transports du Québec, Québec, Canada, 63 p.

Siegel, D.A., Maritorena, S., Nelson, N.B., Hansell, D.A. et Lorenzi-Kayser, M. (2002). Global distribution and dynamics of colored dissolved and detrital organic materials, *Journal of Geophysical Research-Oceans, 107*(C12), 3228

Smith, A., Delavau, C. et Stadnyk, T. (2015). Identification of geographical influences and flow regime characteristics using regional water isotope surveys in the lower Nelson River, Canada, *Canadian Water Resources Journal/Revue canadienne des ressources hydriques*, *40*, 23-35.

Song, G., Li, Y., Hu, S., Li, G., Zhao, R., Sun, X. et Xie, H. (2017). Photobleaching of chromophoric dissolved organic matter (CDOM) in the Yangtze River estuary: kinetics and effects of temperature, pH, and salinity, *Environmental Science: Processes & Impacts*, *19*, 861-873.

Song, G., Yang, F., Massicotte, P., Wei, H. et Xie, H. (2023). CDOM spectral slope ($S_{275–295}$) as tracers of water masses, CDOM heterogeneity, and Δ^{14}C-DOC in an oligotrophic marginal sea, *Limnology and Oceanography Letters, 8*(5), 789-798.

Spencer, R.G., Ahad, J.M., Baker, A., Cowie, G.L., Ganeshram, R., Upstill-Goddard, R.C. et Uher, G. (2007). The estuarine mixing behaviour of peatland derived dissolved organic carbon and its relationship to chromophoric dissolved organic matter in two North Sea estuaries (UK), *Estuarine, Coastal and Shelf Science*, *74*, 131-144.

Spencer, R.G., Aiken, G.R., Butler, K.D., Dornblaser, M.M., Striegl, R.G. et Hernes, P. J. (2009). Utilizing chromophoric dissolved organic matter measurements to derive export and reactivity of dissolved organic carbon exported to the Arctic Ocean: A case study of the Yukon River, Alaska, *Geophysical Research Letters*, *36*, L06401.

Spencer, R.G., Aiken, G.R., Dornblaser, M.M., Butler, K.D., Holmes, R.M., Fiske, G., Mann, P.J. et Stubbins, A. (2013). Chromophoric dissolved organic matter export from US rivers, *Geophysical Research Letters*, *40*, 1575-1579.

Stedmon, C. et Markager, S. (2001). The optics of chromophoric dissolved organic matter (CDOM) in the Greenland Sea: An algorithm for differentiation between marine and terrestrially derived organic matter, *Limnology and Oceanography*, *46*, 2087-2093.

Stedmon, C.A., Amon, R.M.W., Rinehart, A.J. et Walker, S.A. (2011). The supply and characteristics of colored dissolved organic matter (CDOM) in the Arctic Ocean: Pan Arctic trends and differences, *Marine Chemistry*, *124*, 108-118.

Stubbins, A., Hubbard, V., Uher, G., Law, C.S., Upstill-Goddard, R.C., Aiken, G.R. et Mopper, K., (2008). Relating carbon monoxide photoproduction to dissolved organic matter functionality, *Environmental science & technology*, *42*(9), 3271-3276.

Taha, W., Bonneau-Lefebvre, M., Cueto Bergner, A. et Tremblay, A. (2019). Evolution from past to future conditions of fast ice coverage in James Bay, *Frontiers in Earth Science*, *7*, 254.

Thibault, S. et Payette, S. (2009). Recent Permafrost Degradation in Bogs of the James Bay Area, Northern Quebec, Canada, *Permafrost and Periglacial processes*, *20*, 383-389.

Twardowski, M.S. et Donaghay, P.L. (2002). Photobleaching of aquatic dissolved materials: Absorption removal, spectral alteration, and their interrelationship, *Journal of Geophysical Research*, *107*(C8), 3091.

Twardowski, M.S., Boss, E., Sullivan, J. M. et Donaghay, P.L. (2004). Modeling the spectral shape of absorbing chromophoric dissolved organic matter, *Marine Chemistry*, *89*, 69–88.

Vincent, J.S. (1977). Le quaternaire récent de la région du cours inférieur de La Grande Rivière, Québec, *Commission géologique du Canada*, *76*(19), 20 p.

Vodacek, A., Blough, N.V., DeGrandpre, M.D., Peltzer, E.T. et Nelson R. K. (1997), Seasonal variation of CDOM and DOC in the Middle Atlantic Bight: Terrestrial inputs and photooxidation, *Limnology & Oceanography*, *42*, 674–686.

Weishaar, J.L., Aiken, G.R., Bergamaschi, B.A., Fram, M.S., Fujii, R. et Mopper, K. (2003). Evaluation of specific ultraviolet absorbance as an indicator of the chemical composition and reactivity of dissolved organic carbon, *Environmental Science & Technology*, *37*, 4702-4708.

Wells, M.L. (2002). Marine colloids and trace metals. Dans: Hansell, D.A. et Carlson, C.A., Eds., Biogeochemistry of Marine Dissolved Organic Matter, Academic Press, San Diego, CA, USA, 367-404.

Wologo, E., Shakil, S., Zolkos, S., Textor, S., Ewing, S., Klassen, J., Spencer, R.G.M., Podgorski, D.C., Tank, S.E., Baker, M.A., O'Donnell, J.A., Wickland, K.P., Foks, S.S.W., Zarnetske, J.P., Lee-Cullin, J., Liu, F., Yang, Y., Kortelainen, P., Kolehmainen, J., Dean, J.F., Vonk, J.E., Holmes, R.M., Pinay, G., Powell, M.M., Howe, J., Frei, R.J., Bratsman, S.P., Abbott, B.W. (2021). Stream Dissolved Organic Matter in Permafrost Regions Shows Surprising Compositional Similarities but Negative Priming and Nutrient Effects, *Global Biogeochemical Cycles*, *35*, e2020GB00671.

Xenopoulos, M.A., Barnes, R.T., Boodoo, K.S., Butman, D., Catalán, N., D'Amario, S.C., Fasching, C., Kothawala, D.N., Pisani, O. et Solomon, C.T. (2021). How humans alter dissolved organic matter composition in freshwater: Relevance for the Earth's biogeochemistry, *Biogeochemistry*, *154*, 323-348.

Xie, H., Aubry, C., Bélanger, S. et Song G. (2012). The dynamics of absorption coefficients of CDOM and particles in the St. Lawrence estuarine system: Biogeochemical and physical implications, *Marine Chemistry, 128*, 44-56.

Xie, H., Aubry, C., Zhang, Y. et Song, G. (2014). Chromophoric dissolved organic matter (CDOM) in first-year sea ice in the western Canadian Arctic, *Marine Chemistry*, *165*, 25-35.

Zepp, R.G., 2003. Solar UVR and aquatic carbon, nitrogen, sulfur and metals cycles. Dans: Helbling, E.W., Zagarese, H. (Eds.), UV Effects in Aquatic Organisms andEcosystems, The Royal Society of Chemistry, Cambridge, UK, 137–184.

Zhang, Y., Xie, H. et Chen, G. (2006). Factors affecting the efficiency of carbon monoxide photoproduction in the St. Lawrence estuarine system (Canada), *Environmental Science & Technology*, *40(*24), 7771-7777.

Zhang, Y. et Xie, H. (2015). Photomineralization and photomethanification of dissolved organic matter in Saguenay River surface water, *Biogeosciences*, *12*(22), 6823–6836.